Stem Cell Research (2013) 11, 634–646

Available online at www.sciencedirect.com

SciVerse ScienceDirect

www.elsevier.com/locate/scr

Neonatal mesenchymal-like cells adapt to surrounding cells

Stefanie Liedtke [a,*,1], Eva Maria Freytag [a,1], Julia Bosch [a], Amelie Pia Houben [a], Teja Falk Radke [a], René Deenen [b], Karl Köhrer [b], Gesine Kögler [a]

[a] *Institute for Transplantation Diagnostics and Cell Therapeutics, Heinrich-Heine-University Medical Center, Düsseldorf, Germany*
[b] *Biological and Medical Research Center (BMFZ), Heinrich-Heine-University, Düsseldorf, Germany*

Received 2 October 2012; received in revised form 22 March 2013; accepted 2 April 2013

Abstract Hematopoietic cord blood (CB) transplantations are performed to treat patients with life-threatening diseases. Besides endothelial cells, the neonatal multipotent stromal cell subpopulations CDSCs (CB-derived stromal cells) and USSCs (unrestricted somatic stromal cells) are like bone marrow (BM) SCs interesting candidates for clinical applications if detailed knowledge is available. Clonal USSC compared to CDSC and BMSC lines differ in their developmental origin reflected by a distinct *HOX* expression. About 20 (out of 39) *HOX* genes are expressed in CDSCs (HOX+), whereas native USSCs reveal no *HOX* gene expression (HOX-). Moreover, USSCs display a lineage-specific absence of the adipogenic differentiation potential. As the specific HOX code can be ascribed to topographic bodysites it may be important to match the HOX code of transplanted cells to the tissue of interest. Herein co-culture experiments were performed, presenting a novel approach to modulate the differentiation potency of USSCs towards HOX positive stromal cells. After co-culturing native USSCs with CDSCs and BMSCs, USSCs adapt a positive HOX code and gain the adipogenic differentiation capacity. These results present for the first time modulation of a lineage-specific differentiation potential by co-culture. Finally, USSCs can be claimed as potential candidates to substitute unique progenitor cell populations in clinical approaches.

Introduction

Besides hematopoietic stem cells (HSCs), multipotent stromal cells are claimed to be a promising source for clinical applications, but their typical differentiation capacities depending on their origin (cord blood, CB; bone marrow, BM; adipose tissue, AT) might have an impact on their usefulness in specific clinical applications. Therefore, a detailed characterization of their developmental origin and their lineage-specific differentiation potential is mandatory to elaborate, if a specific cell source might be favourable for bone and cartilage formation. Questionable as well is, if mixed bulk cultures should be applied in clinical applications, as no detailed knowledge is available on the impact of mixed subpopulations of stromal cells. In cord blood, two distinct clonal neonatal subpopulations are described: USSCs (unrestricted somatic stromal cells) and CDSCs (cord blood derived stromal cells) (Kluth et al., 2010; Kogler et al., 2004; Liedtke et al., 2010). Regarding their immunophenotype both clonal neonatal cell types share the same pattern of

Abbreviations: CB, cord blood; BM, bone marrow; CD, cord blood derived; SCs, stromal cells; USSCs, unrestricted somatic stromal cells; UC, umbilical cord

* Corresponding author at: Institute for Transplantation Diagnostics and Cell Therapeutics, Heinrich-Heine-University Medical Center, Moorenstrasse 5, D-40225 Düsseldorf, Germany. Fax: +49 211 8104340.
E-mail address: liedtke@itz.uni-duesseldorf.de (S. Liedtke).
[1] Authors contributed equally.

1873-5061/$ - see front matter © 2013 Elsevier B.V. All rights reserved.
http://dx.doi.org/10.1016/j.scr.2013.04.001

surface molecules ($CD45^-$, $CD13^+$, $CD29^+$, $CD73^+$, $CD105^+$) similar to bone marrow-derived stromal cells (Erices et al., 2002) and are commonly referred to as "MSCs" phenotype (Dominici et al., 2006). However, the markers used to describe stromal cells are not specific and are expressed by many connective tissue cells that are not stem cells. To date, a marker set clearly distinguishing connective tissue stem cells from more mature cells is not available. As the term "MSCs", which can stand for mesenchymal stromal cells as well as multipotent stromal cells, is controversially discussed (Bianco, 2011a), we will refer to cells derived out of cord blood (CDSCs and USSCs) and out of bone marrow (BMSCs) as stromal cells in this paper.

A great advantage of these CDSCs and USSCs is their simple isolation and expansion *in vitro*. Likewise, USSCs produce functionally significant amounts of hematopoiesis-supporting cytokines and are superior to BMSCs in expansion of $CD34^+$ cells from cord blood (Kogler et al., 2005). USSCs are therefore a suitable candidate for stroma-driven *ex vivo* expansion of hematopoietic cord blood cells for short-term reconstitution or co-transplantation (Jeltsch et al., 2011). In the near future, these cells may be applied to patients to reduce the graft-versus-host disease, the most occurring side effect after transplantation of hematopoietic stem cells or to support hematopoiesis (Abdallah and Kassem, 2009). USSCs and CDSCs share the osteogenic and chondrogenic differentiation potential. In a recent study our group analysed in detail the expression of osteogenic and chondrogenic marker genes during differentiation defining the osteogenic signature of USSCs, CDSCs, BMSCs and (umbilical cord) UCSCs (Bosch et al., 2012). Based on the work of Kluth et al. (2010), it was demonstrated that USSCs in contrast to CDSCs do not differentiate naturally towards the adipogenic lineage, while expressing the adipogenic inhibitor *Delta-like 1 homolog* (*DLK1*) on a transcript but not on a secreted protein level. In addition, expression of *HOX* genes is absent in USSCs, whereas CDSCs revealed a typical positive *HOX* code similar to BMSCs (Liedtke et al., 2010).

HOX genes are essential for normal development of vertebrates by determining the positional identity along the anterior-posterior body axis (Krumlauf, 1994). In humans, the 39 known *HOX* genes are distributed among four paralogous clusters *HOXA* to *HOXD*, located in chromosomes 7, 17, 12 and 2, respectively. *HOX* genes are expressed sequentially 3´ to 5´ along the body axis during embryogenesis, termed "temporal and spatial colinearity" (Kmita and Duboule, 2003). The typical *HOX* code of a cell describes the specific expression of functional active *HOX* genes in distinct tissues (Gruss and Kessel, 1991). More importantly *HOX* genes may also have a therapeutic application in near future. It was found that HOXD3 protein is upregulated during normal wound repair (Hansen et al., 2003). The protein promotes angiogenesis and collagen synthesis, but is absent in poorly healing wounds of genetically diabetic mice. After adding HOXD3, the treatment resulted in faster diabetic wound closure and tissue remodeling.

While the facial skeleton is formed by HOX negative neural crest cells (Creuzet et al., 2002), the skeleton, originating from mesoderm-derived progenitor cells, is usually HOX positive in adults (Leucht et al., 2008). In bone regeneration experiments, Leucht et al. revealed that the HOX negative mandibular progenitor cells are favourable in bone repair as compared to the HOX positive tibial progenitor cells (Leucht et al., 2008). In their experiments, HOX negative mandibular progenitor cells started to express *HOX* genes after transplantation into a tibial bone defect leading to bone repair. In contrast to that, HOX positive tibial progenitor cells transplanted into a mandibular defect failed to regenerate bone. This data is supported by recent findings, suggesting the biological advantages of HOX negative cells isolated from endoral sites (Lohberger et al., 2012). The potency of a HOX negative cell to adapt the HOX code of surrounding cells or tissues therefore seems to be an important feature for regenerative approaches but also for the normal development in the skeleton of the fetus.

As *HOX* genes are able to translocate passively through biological membranes, a technique applying a co-culture method provides several advantages. In the work presented here, USSCs (HOX^-) with a restricted adipogenic potential were co-cultured with CDSCs and BMSCs (HOX^+) to test if the USSCs are able to adapt a *HOX* positive expression pattern. Additionally, changes of the lineage-specific cell fate modulated by co-culture were monitored for osteogenic, chondrogenic and adipogenic differentiation in this approach. Finally, following hypotheses were tested:

Do USSCs have the potential to adapt the *HOX* expression pattern of a surrounding celltype?
Can the differentiation capacity be switched to an adipogenic direction by exposing USSCs to *HOX* positive CDSCs able to generate adipocytes?
Is the osteogenic differentiation capacity of USSCs affected by co-culture with CDSCs and BMSCs?
Can USSCs be claimed as potential candidates to substitute unique progenitor cell populations?

Material and methods

Generation and expansion of CB-derived cells and BMSCs

USSCs and CDSCs were generated as described previously (Bosch et al., 2012; Kluth et al., 2010). In brief, CB was collected from the umbilical cord vein with informed consent of the mother. Mononuclear cells (MNC) were obtained by ficoll (Biochrom, density 1.077 g/cm^3) gradient separation followed by ammonium chloride lysis of RBCs. 5–7 *10^6 CB MNC/ml were cultured in DMEM low glucose (Cambrex) with 30% FCS (Perbio), 10^{-7} M dexamethasone (Sigma-Aldrich), penicillin/streptomycin and L-glutamine (PSG; Cambrex). Clonal populations were obtained from cord blood by applying special cloning cylinders. Cell lines were generated as described before and, as soon as distinct, separate colonies were observed, a cloning cylinder was attached on a single colony and cells were trypsinated according to the standard protocol. BMSCs were isolated using BM aspirated from the iliac crest of healthy unrelated donors as previously described (Kluth et al., 2010).

Transfection of USSCs

The transfection of USSCs was performed using the transfection reagent FuGENE® (Roche Applied Science, Mannheim, Germany). The production of lentiviral particles

was accomplished by transfection of HEK293T cells with three plasmids: envelope plasmid GALV TM, helper plasmid pCD/NL-BH and the expression vector pCL6IEGwo containing the eGFP sequence (Supplementary Fig. 1). The transfection was done according to following protocol: Day 1: HEK293T cell splitting 5 * 10^6 cells/10 cm Ø cell plate in DMEM (high glucose), 10% FCS, 1% PSG. Day 2: HEK293T transfection: DMEM (high glucose) + 5 μg of each plasmid DMEM (high glucose) + 45 μl FuGENE® were mixed and incubated for 15 min at room temperature and added to HEK293T cultures in DMEM (high glucose), 5% FCS, 1% Glutamin. Day 3: Target cells were thawed (1 * 10^5 cells/six-well plate), HEK293T culture medium was exchanged with DMEM (high glucose), 5% FCS, 1% PSG. Day 4: Infection of target cells: Extracellular supernatant containing virus particles from HEK293T cultures was sterile filtered (0.45 μm filter) and added to target cells (pure and 1:4 diluted). Day 5: Medium change of target cells (DMEM (low glucose), 30% FCS, 1% PSG).

Cell sorting

Cells with a high eGFP expression were sorted after transfection if the percentage of eGFP-expressing cells was below 85%. After discarding the supernatant, the cells were washed twice with PBS/0.5% HSA and resuspended in 750 μl PBS/0.5% HSA. The sorting was performed with a high speed sorter MoFLo XDP (Beckman–Coulter) in the Core Flow Cytometry Facility of the ITZ. After sorting cells were plated on cell dishes for at least 24 h before analysis.

Co-culture experiments

For co-culture experiments, the same amount of USSCs and CD/BMSCs was cultivated in one flask in normal cultivation medium (DMEM (low glucose: 1 g/l), 30% FCS, 1% Penicillin/Streptomycin, 1% L-glutamine) for 16 h or 5 days. To separate the USSCs from CD/BMSCs, the USSCs were sorted via eGFP-expression. A stringent sorting gate was applied ensuring that 10% of highly GFP expressing cells were sorted (Supplementary Fig. 2A). Reanalysis of sorted cells revealed a purity of cells >98% (Supplementary Fig. 2B). After 24 h subsequent to sorting, RNA was isolated for analysis of the gene expression via PCR and Primeview Affymetrix Arrays. After further passages (P) subsequent to sorting, the cells were differentiated into adipogenic (1P and 3P), chondrogenic (1P) and osteogenic (1P) direction. In the Supplementary Fig. 3 schematical procedure of co-culture experiments and subsequent analyses is depicted.

In vitro differentiation

USSCs, CDSCs and BMSCs were differentiated as described previously (Bosch et al., 2012; Kluth et al., 2010). In brief, for adipogenic differentiation the differentiation medium was replaced twice a week, alternating induction (containing dexamethasone, indomethacine, insuline and 3-Isobutyl-1methylxantin) and cultivation medium (containing insulin). To visualize the lipid vacuoles, the differentiated cells were fixed with formaldehyde (4 °C, 20 min) and stained with oil red O (Sigma Aldrich).

For chondrogenic differentiation, the pelleted cells were incubated for 21 days in medium containing dexamethasone, ascorbic-acid-2-phosphate, sodium pyruvate, insulin-transferrin-selenium and TGFbeta1. The media were changed twice a week. For Safranin O/Fast Green (Waldeck) following standard protocol, the pellets were cut into sections of 6 mm using a cryotom after being embedded in Tissue Freezing Medium (Jung, Leica).

For osteogenic differentiation the medium containing sodium L-ascorbate, β-glycerolphosphate disodium salt hydrate and dexamethasone was changed twice a week for 14 days. To detect mineralization, the differentiated cells were fixed with cold ethanol (70%, 10 min) and stained with Alizarin Red S-(Sigma-Aldrich) according to standard protocols. For quantification of Alizarin red 800 μl of 10% acetic acid were added and incubated for 30 min while shaking. The cells were detached with a cellscraper and transferred to a 1.5 ml eppendorf tube. Samples were vortexed for 30 s then heated at 85 °C for 10 min and finally cooled down on ice for 5 min. After a centrifugation step at 24,500 ×*g* for 15 min 500 μl of the supernatant were mixed with 200 μl of 10% ammoniumhydroxide and photometrically measured in a platereader (Bio-Tek Instruments Inc.) at 405 nm. Values of the respective negative control were subtracted from differentiated cells.

Total RNA extraction and reverse transcription

Total RNA was extracted from cell lines and cell samples in a 40 μl volume applying the RNeasy Kit (Qiagen) according to the manufacturer's instructions. Determination of RNA concentrations was carried out by applying a Nanodrop device (NanoDropTechnologies). Reverse transcription was performed for 1 h at 50 °C using the First-strand cDNA Synthesis Kit (Invitrogen) and the enclosed oligo(dT)20 primer. About 1000 ng total RNA was converted into first-strand cDNA in a 20 μl reaction. All control reactions provided with this system were carried out to monitor the efficiency of cDNA-synthesis. Prior to PCR, the completed first-strand reaction was heat-inactivated at 85 °C for at least 10 min. Finally, cDNA was treated with RNaseH according to the manufacturer's protocol.

RT-PCR and qPCR

RT-PCR was carried out with intron-spanning primers specific for each *HOX* gene (Liedtke et al., 2010) (Thermo Scientific). Either *RPL13A* or *GAPDH* was used as reference gene for normalization. Approximately 15 ng of cDNA was used for subsequent RT-PCR-analysis in a total volume of 25 μl containing 1× PCR buffer, 0.2 μM of each primer, 1.5 mM $MgCl_2$, 0.2 mM each dNTP and 1 U *Taq* DNA Polymerase (Invitrogen) at the following conditions: (1) 2 min at 95 °C for initial denaturation and *Taq* Polymerase activation, (2) 30 s at 95 °C, 30 s at 56 °C, (3) 30 s at 72 °C for 35 cycles, 5 min at 72 °C for final extension of PCR products. PCR was performed on a Mastercycler ep gradient S (Eppendorf). Subsequently, aliquots of the RT-PCR products and related controls were analysed on a 2% agarose gel by electrophoresis. qPCR was carried out with SYBR® Green PCR Mastermix (Applied Biosystems) using 50 ng template cDNA. All reactions were run in duplicates/triplicates, respectively, on a Step One Plus

(Applied Biosystems). The sequences for primers (Supplementary Table. 1) were carefully examined and checked for their specificity. Relative changes in gene expression were calculated following the ΔΔCt-method with *GAPDH* or *RPL13A* as internal standard. Relative gene expression was illustrated as mean values.

Immunocytochemistry

Immunocytochemical staining was performed using an antibody to human HOXC10 protein (Abnova, 1:250 dilution). Secondary antibody (Rhodamine Red X-conjugated AffiniPure Goat-Anti-Mouse IgG; Jackson Immunoresearch) was applied in a 1:2000 dilution. For enhancement of the native GFP-signal the anti GFP rabbit IgG antibody conjugated with Alexa Fluor 488 (Life technologies) was applied 1:250. All photographs were taken under the same parameters with a confocal Zeiss LSM 700 microscope and ZEN 2011 software.

Microarray Gene Expression Analyses

Cell lines used for Microarray Gene Expression Analyses were cultured for 4 days. Total RNA was extracted on day 4 according to the RNeasy Mini Kit protocol (Qiagen). RNA preparations were checked for RNA integrity by Agilent 2100 Bioanalyzer. All samples in this study showed high quality RNA Integrity Numbers (RIN) of 10. RNA was quantified by photometric Nanodrop measurement.

Synthesis of cDNA and subsequent biotin labelling of cRNA was performed according to the manufacturers' protocol (3´ IVT Express Kit; Affymetrix, Inc.). Briefly, 100 ng of total RNA was converted to cDNA, followed by *in vitro* transcription and biotin labelling of aRNA. After fragmentation labelled aRNA was hybridized to Affymetrix PrimeView™ Human Gene Expression Microarrays for 16 h at 45 °C, stained by streptavidin/phycoerythrin conjugate and scanned as described in the manufacturer's protocol.

Data analyses on digitized fluorescence signal intensities were conducted with GeneSpring GX software (Vers. 12.1; Agilent Technologies). Probes within each probeset were summarized by RMA after quantile normalization of probe level signal intensities across all samples to reduce inter-array variability (Bolstad et al., 2003). Input data pre-processing was concluded by baseline transformation to the median of all samples.

After grouping of samples according to their respective experimental condition (USSC d0, USSC 16 h and USSC 5 d, three replicates each) a given probeset had to be expressed above background (i.e. fluorescence signal of a given probeset was detected within the 20th and 100th percentiles of the raw signal distribution of a given array) in at least 66% of replicates in any one of three groups to be further analysed. Differential gene expression was statistically determined by ANOVA analysis ($p < 0.05$), followed by FDR correction for multiple testing (Benjamini–Hochberg).

Annotation Lists containing 278 differentially expressed probeset IDs were subjected to the "Functional Annotation Cluster Tool" provided by DAVID Bioinformatics Resources (http://www. david.abcc.ncifcrf.gov/) (Dennis et al., 2003; Huang da et al., 2009; Sherman et al., 2007).

Results

Co-cultivation of USSCs with either CDSCs or BMSCs leads to the expression of *HOX* genes.

In a first approach, it was hypothesized that *HOX* negative USSCs might have the potential to adapt the *HOX* code from surrounding cells, as it was described in mice by Leucht et al. for mandibular periosteal cells (*HOX*$^-$), expressing *HOX* genes after co-culture with tibial periosteal cells (*HOX*$^+$) (Leucht et al., 2008). CDSCs display a neonatal subpopulation differing from USSCs by their positive HOX code. Therefore, we decided to use this neonatal model system as it is likely that these celltypes come in close contact *in vivo*. A transwell system was applied to test this hypothesis. USSCs were co-cultured for 5 days with a CDSC line in the transwell insert. Afterwards *HOX* gene expression in USSCs was tested by conventional reverse transcriptase PCR (RT-PCR). In none of the experiments performed, USSCs developed a positive *HOX* expression pattern (data not shown here). Thereby it can be excluded that possible interactions affecting the *HOX* expression applying transwells occur through soluble factors such as cytokines or exosomes.

Supposing that direct cell-cell contacts are necessary to manipulate neonatal *HOX*$^-$ USSCs, a direct co-culture system was tested. In previous experiments several titrations of USSCs with CDSCs were performed to exclude possible PCR artefacts caused by residual CDSCs cells after sorting. CDSCs cells were diluted with USSCs in a ratio of 1:1000, 1:100, 1:50 and 1:20 (Supplementary Fig. 4). After RT PCR, none of the 39 *HOX* genes tested could be observed in the 1:100 dilution and only 2–3 of the most highly expressed *HOX* genes were observed at a low level in the 1:50 and the 1:20 dilution. This result clearly demonstrates that except for rare weak signals most likely deriving from highly expressed *HOX* genes, no other *HOX* genes can be detected even if 5% of *HOX* positive cells are present. In the following experiments, GFP-labelled USSC lines were applied and strictly sorted subsequently by fluorescence activated cell sorting (FACS) after co-cultivation with either CDSCs or BMSCs. By an extremely stringent sorting strategy we minimized the possibility of interfering contamination to less than 2% (Supplementary Fig. 2). Fig. 1 depicts exemplary results of the first direct co-culture experiments. In Fig. 1A, the *HOX* gene expression patterns of all native cell lines analysed in the following experiments are illustrated. Individual USSC lines tested revealed *HOX* gene expression after direct co-culture for 5 days with either CDSCs or BMSCs (Fig. 1B). The most abundant genes detected after co-culture were the paralogous genes *HOXA10*, *HOXC10* and *HOXD10*. However, USSCs did not completely adapt the identical *HOX* code of the co-cultivated cell line after 5 days of co-culture. These results were confirmed on protein level by immunocytochemistry for one of the most abundant *HOX* gene *HOXC10* (Fig. 2). This mandatory experiment proves that USSC without co-culture display no HOXC10 expression on protein level, whereas after co-culture, the HOXC10 protein was clearly detectable in GFP-expressing cells.

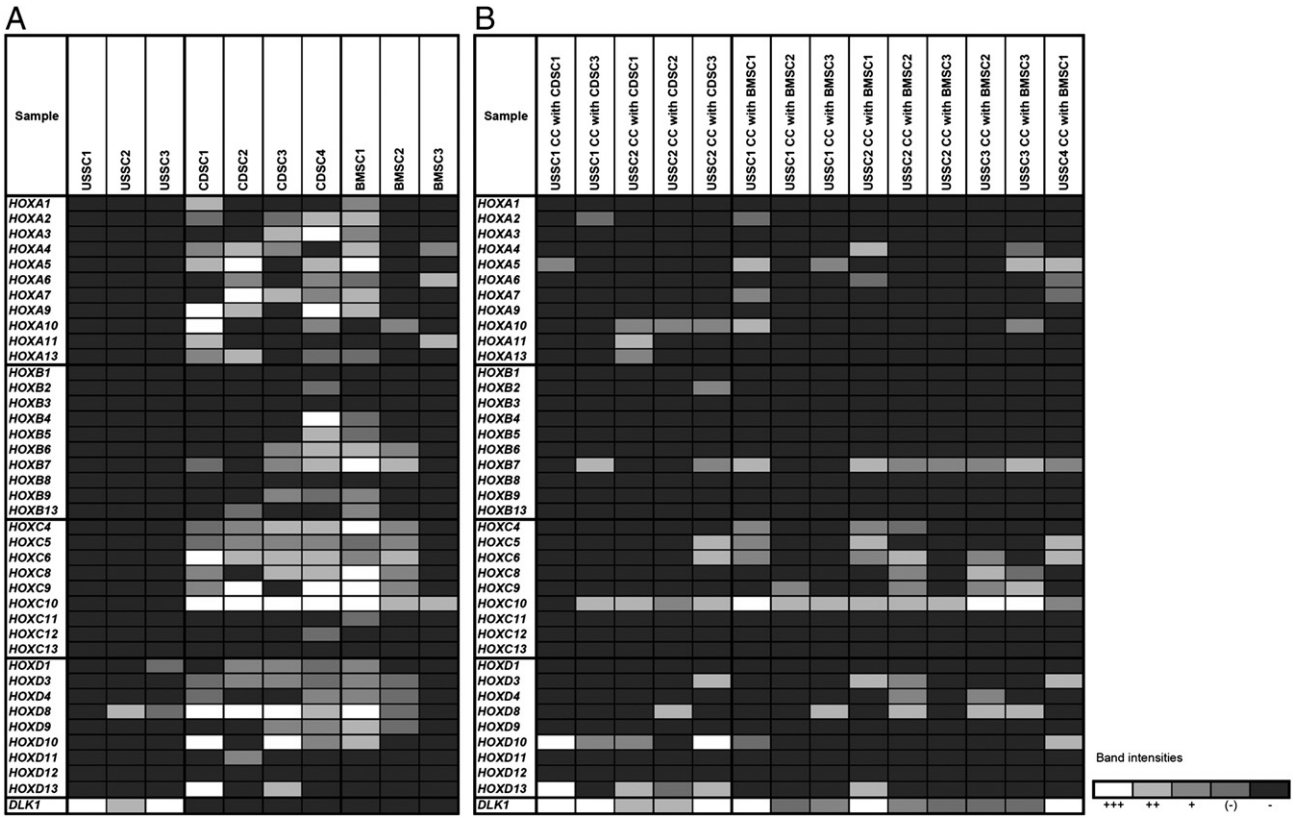

Fig. 1 Native *HOX* negative USSC lines revealed *HOX* gene expression after 5 days of co-cultivation with *HOX* positive cell types. A: The *HOX* gene expression patterns of all cell lines used in co-culture experiments were measured by RT-PCR. Intensity of product bands was judged from negative "−" to strongly positive "+++" in a graduated manner (for examples see legend) and visualized by a heat map. B: USSCs co-cultivated for 5 days with either CDSCs or BMSCs were sorted by FACS and subsequently tested for the expression of 39 *HOX* genes and adipogenesis inhibitor *DLK1* by RT PCR.

Thereby the results presented on transcript level were validated on protein level demonstrating within one single cell co-expression of both markers.

In order to determine if USSCs can be manipulated by other different *HOX* positive cell populations as well, the osteosarcoma cell line SAOS-2 was co-cultivated with USSCs to test this hypothesis. Supplementary Fig. 5A reveals that USSC lines (n = 2) were able to express *HOX* genes after co-culture with SAOS-2 cells whereas the most abundant *HOX* genes were *HOXC10* and *HOXD10*. The significance of these results displays that generally co-cultivation of cells might impact the *HOX* gene expression pattern of cells and confirms the adaptiveness of USSCs to surrounding cells. In order to test if other HOX negative cells harbour the same adaptiveness, co-cultures of CDSCs with *HOX* negative cells derived from the human mandibular bone were performed as a biological control. Except for *HOXD3*, the mandibular bone cells did not express additional *HOX* genes after this co-culture experiment (Supplementary Fig. 5B). We expected to get *HOX* gene expression in mandibular progenitor cells, as it was described by Leucht et al. (2008) in mice, however, we cannot rule out, that the cells we generated from the mandibular bone display more fibroblastic cells instead of real progenitor cells explaining this discrepancy. Moreover, one important conclusion we can draw from this experiment is, that contamination of residual CDSCs was sufficiently minimized, as no additional *HOX* gene was detectable in co-cultured mandibular cells after sorting the cells by flow cytometry.

In the following experiments it was tested if the developed *HOX* code can be maintained during longtime

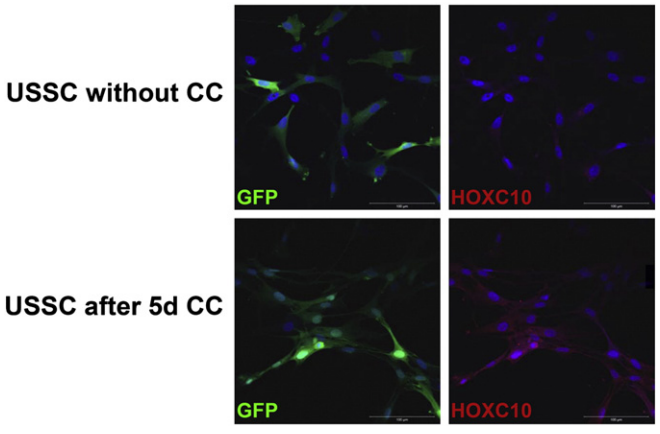

Fig. 2 Co-staining of HOXC10 and GFP protein in USSCs after co-culture with CDSCs. USSC2 was co-cultivated (CC) with CDSC1 for five days, sorted via FACS and plated on chamber slides for immunohistochemical staining. All photographs were taken under the same parameters with a Zeiss LSM 700 Microscope applying the ZEN 2011 software. The scale is 100 μm.

cultivation without a continuous trigger of the co-cultivated cell line. Therefore, after 5 days of co-culture (with either CDSCs or BMSCs) sorted USSCs were cultivated for up to three additional passages and *HOX* gene expression was evaluated in subsequent passages. RT-PCR revealed an even higher amount of expressed *HOX* genes after subsequent passaging of USSCs (Supplementary Fig. 5C). Either, the existent *HOX* gene expression increased or other *HOX* genes were newly expressed. In all experiments *HOXB7*, *HOXC10* and *HOXD10* seem to be the most stably expressed genes. Interestingly, the amount of the adipogenic inhibitor *DLK1* transcript decreased by subsequent passaging and was finally absent in USSCs co-cultivated with CDSCs after three additional passages.

Taken together these preliminary results have proven that USSCs harbour the potential to develop a positive *HOX* code which is not attenuated in later passages. Moreover, the downregulation of the adipogenic inhibitor *DLK1* in later passages indicates that the adipogenic potential of USSCs might have been affected by the co-culture experiment.

USSCs develop an adipogenic differentiation potential after co-culture with CDSCs.

In contrast to CDSC and BMSC lines, native USSCs are *HOX* negative and possess no adipogenic differentiation potential. In order to define if co-cultivated USSCs (*HOX*$^+$) which downregulate the adipogenic inhibitor *DLK1* are able to modulate their differentiation capacity, cells were differentiated into the adipogenic lineage after 5 days of co-culture with CDSCs and BMSCs. After 21 days of adipogenic differentiation the cells were stained with Oil-Red O for visualisation of lipid vacuoles (Fig. 3A). Fig. 3A demonstrates the ability of USSCs to generate lipid vacuoles after co-culture with a CDSC line for 5 days when adipogenic differentiation was started 1 passage after sorting. The resulting stainings clearly uncovered lipid vacuoles in USSCs after co-culture. In the USSC d0 control without co-culture no lipid vacuoles were detectable. It is very unlikely that lipid vacuoles detectable in such a high amount of cells result from residual CDSCs, as further proliferation is strongly restricted by induction of adipogenesis. The adipogenic differentiation was likewise started 3 passages after sorting and revealed the same result (Supplementary Fig. 6). Less lipid vacuoles could be detected whereas in the d0 control no staining was visible supporting the hypothesis that the adipogenic differentiation potential of USSCs can be modulated by co-culture. The reduction of the adipogenic ability can most likely be ascribed to the extended passaging, as this is a common observation in CDSCs and USSCs in long term culture. To confirm these results, the adipogenic marker *Adipocyte, C1Q and collagen domain containing* (*ADIPOQ*), and the adipogenic inhibitor *Delta-like 1 homolog* (*DLK1*) were tested (Fig. 3B). The adipogenic related gene *ADIPOQ* was not significantly regulated directly after co-culture but was highly increased at day 21 of adipogenic differentiation. The adipogenic inhibitor *DLK1* increased directly after co-culture but was completely downregulated after adipogenic differentiation. As we expected the *DLK1* gene to be downregulated directly after co-culture we followed up the expression kinetics of *DLK1* in subsequent passages and tested USSC2 in an independent experiment with one CDSC line and one BMSC line (Supplementary Fig. 7). After subsequent passaging of the USSCs, expression of the adipogenic inhibitor *DLK1* decreased after 5 days of co-culture and was nearly absent after two additional passages.

The chondrogenic and osteogenic differentiation potential of USSCs is affected by co-culture.

To test if the adaption of the *HOX* gene expression has an influence on the chondrogenic and osteogenic differentiation potentials of the USSCs, the co-cultured undifferentiated USSCs were analysed for genes related to the osteogenic/chondrogenic lineage. For the osteogenic differentiation, the markers *Sp7 transcription factor (OSX)*, *integrin-binding sialoprotein* (*BSP*), *bone morphogenetic protein 2* (*BMP2*) and *bone morphogenetic protein 4* (*BMP4*) were used. Besides other bone and cartilage associated genes like *twist homolog 1* (*TWIST1*), *parathyroid hormone-like hormone (PTHLH)*, *runt-related transcription factor 2* (*RUNX2*), *msh homeobox 2* (*MSX2*), and *forkheadbox F1* (*FOXF1*) genes specific for cartilage like *Sry-box 9* (*SOX9*), *collagen 1 A1* (*COL1A1*) and *aggrecan* (*ACAN*) were analysed.

After co-culture of USSCs (n = 3) with CDSCs 10 out of 12 genes tested revealed a differential expression in all three independently measured USSCs (Supplementary Fig. 8). Upregulated genes were *BMP2*, *BMP4*, *PTHLH*, *ACAN* and *FOXF1* and downregulated were *BSP*, *RUNX2*, *SOX9*,*TWIST1* and *MSX2*. We applied a paired t-test to evaluate the statistical significance of the regulation by comparison of three individual USSC lines before and after co-culture. However, only BSP revealed a significant downregulation. Although a clear tendency of regulation was detectable, the p value was not significant in all other cases due to the biological variances between the individual cell lines.

We further wanted to test, if the regulations seen in qPCR experiments in d0 samples have a visual impact on the differentiation capacity of co-cultured USSCs. Therefore, cells were differentiated into the chondrogenic direction in a pellet culture and slices were stained with Safranin O (Fig. 4). In Fig. 4 it is visible that co-cultured USSCs display a less condensed chondropellet structure as compared to the controls without co-culture. Furthermore, the amount of proteoglycans is reduced in co-cultured USSCs reflected by a weaker red staining. It appears that they adapt to the co-cultured CDSC line, as the condensation of the respective chondropellet is less condensed as well.

The adaption of the *HOX* gene expression influencing the osteogenic differentiation potential was further analysed applying a CDSC line with a weaker osteogenic differentiation potential as compared to the three USSC lines used for co-cultivation for 5 days. After co-culture, cells were differentiated into the osteogenic direction for 14 days and subsequently stained with Alizarin Red (Fig. 5A). The staining revealed less calcification in the USSCs after co-culture as compared to the native USSC lines at day 0. The calcification was quantified to better judge the difference of treated cells (Fig. 5B). These results significantly confirm the lower osteogenic differentiation capacity of USSCs after co-culture. As the CDSC line used in this experiment possessed a weaker osteogenic differentiation potential compared to the native USSCs, these results

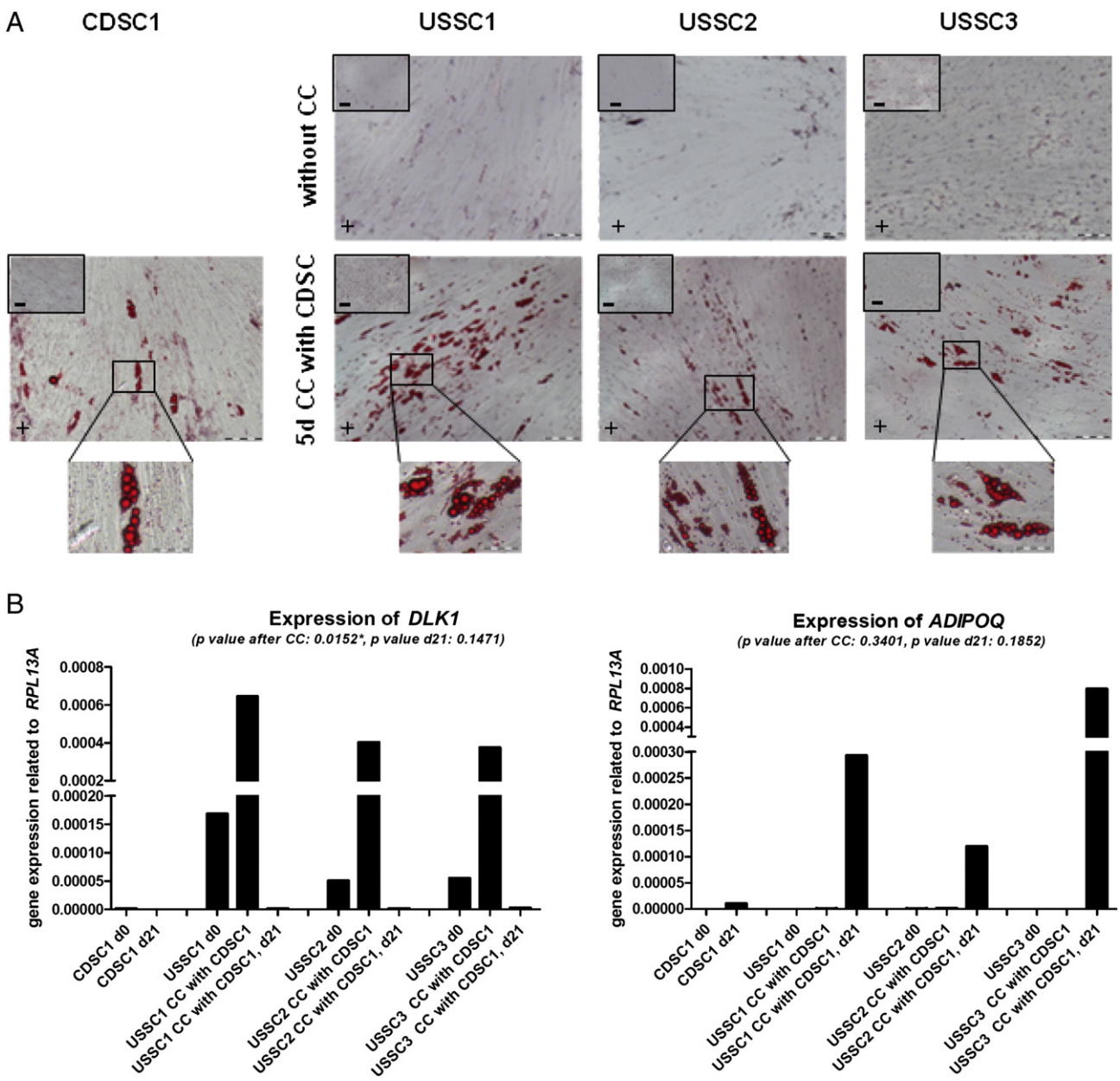

Fig. 3 USSCs reveal an adipogenic differentiation potential after five days of co-culture with CDSCs. A: USSC1-3 were co-cultured (CC) for 5 days with CDSC1. After FACS sort cells were cultivated for 1 further passage and then differentiated into the adipogenic direction for 21 days (d21). Exemplified light microscopic photographs of cells stained with Oil-red-O (detects neutral triglycerides and lipids) at day 21 of adipogenic differentiation in differentiated (+) and control cells (−). Scale bar: 100 μm and 25 μm in the enlarged images. B: qPCR analysis detecting the expression of *DLK1* and *ADIPOQ* at day 0, after 5 days of co-culture (CC) and after co-culture and 21 days of adipogenic differentiation (d21). The gene expression is normalized in relation to *RPL13A*.

support the hypothesis, that USSCs adapt not only the *HOX* code, but moreover adjust their differentiation potentials to surrounding cells.

Affymetrix array analysis revealed further potential candidate genes involved in the modulation of USSCs by co-culture.

In order to define potential candidate genes involved in the modulation of USSCs by co-culture following samples were applied: USSC d0 (n = 3), USSC 16 h after co-culture (n = 3), USSC 5d after co-culture (n = 3). Each USSC line was co-cultivated with the CDSC line hybridized to one additional array (CDSC d0). To first assess differentially expressed genes between the native USSC d0 and co-cultured USSCs after 16 h and 5d, a significance analysis of the array data was accomplished yielding 278 probesets (for a gene list see Supplementary Table 2). Subsequently, the Affymetrix IDs of significantly regulated genes were subjected to a Functional Annotation Cluster analysis (DAVID Bioinformatics Resources 2008 database

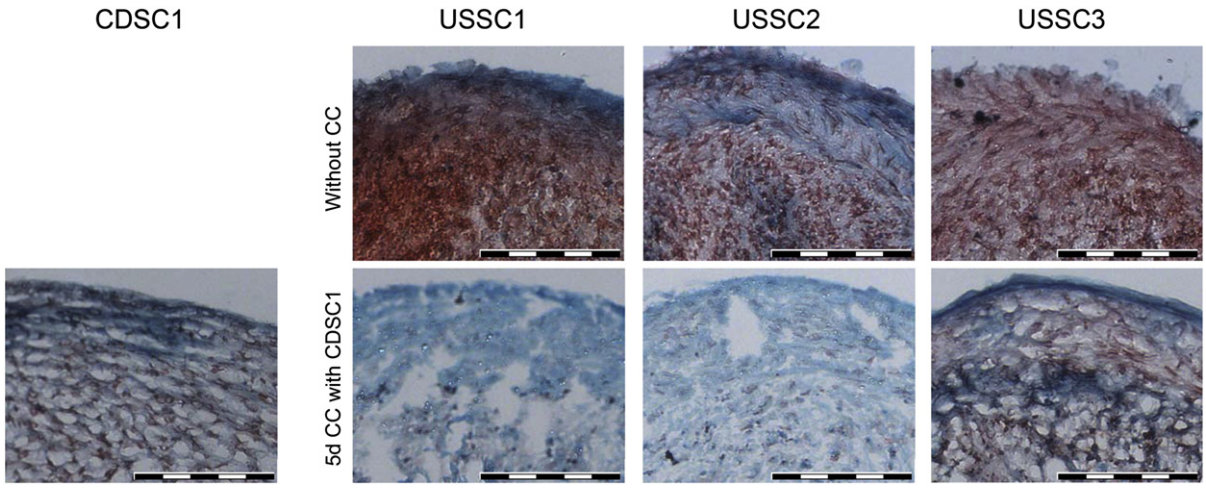

Fig. 4 USSCs showed a chondrogenic differentiation potential before and after co-culture with CDSCs for five days. USSC1-3 were co-cultured (CC) for 5 days with CDSC1, sorted by FACS and afterwards differentiated into the chondrogenic direction for 21 days in a pellet culture. Exemplified light microscopic photographs of safranin O staining. The scale is 100 μm.

http://www.david.abbc.ncifcrf.gov/) (Dennis et al., 2003; Huang da et al., 2009; Sherman et al., 2007). The DAVID Functional Annotation Clustering tool analyses the enrichment of differentially expressed genes in defined functional categories thereby facilitating the biological interpretation in a network context. Analysis outcome revealed Gene Ontology (GO) terms functionally involved in spliceosome/mRNA processing, epigenetic regulation,

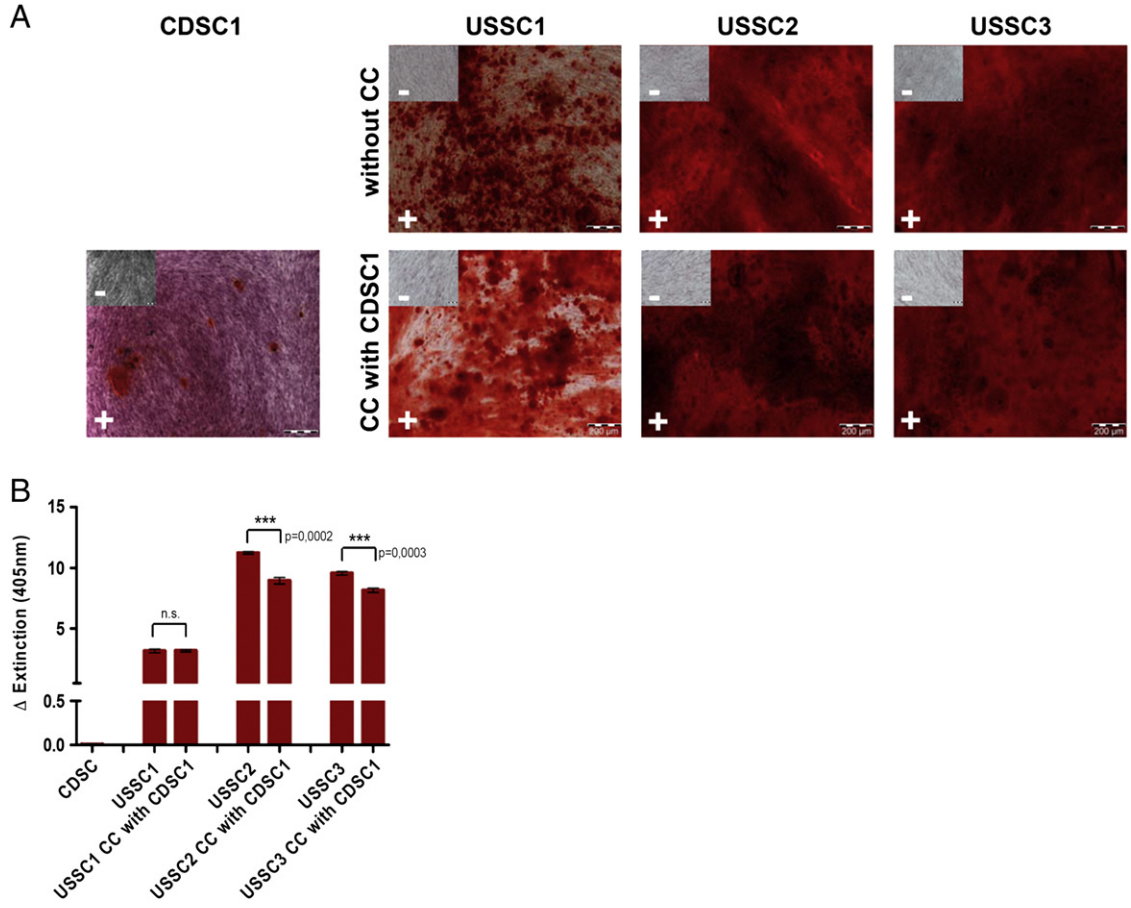

Fig. 5 USSCs co-cultured with CDSCs for 5 days adjusted their osteogenic differentiation potential. A: USSCs were co-cultured for 5 days with CDSCs, sorted by FACS and afterwards differentiated into the osteogenic direction for 14 days. Exemplified light microscopic photographs of cells stained with Alizarin red (detects calcium deposits) were performed at day 14 of osteogenic differentiation. The scale is 200 μm. B: Quantification of Alizarin red was measured in an ELISA reader at 405 nm.

Table 1 Functional Annotation Clustering of differentially expressed genes. A: Annotations related to bone morphogenesis and pattern formation. B: Annotations related to epigenetic regulations. By applying the Affymetrix PrimeView array 278 probeset IDs were found to be significantly differentially expressed in USSC d0 versus USSC 16 h and USSC 5d after co-cultivation with CDSCs. The resulting gene list was further analysed by the DAVID Functional Annotation Clustering Tool to identify gene ontology (GO) terms. This table displays 2 consequential Annotation Clusters of this approach and the respective genes. The count column depicts the amount of genes involved in individual terms. Genes tested are labeled in bold letters.

Gene ontology annotation	Count	P_Value	Benjamini	Genes
A				
Proximal/distal pattern formation	4	3.5OE−03	4.7OE−01	**HOXA10, HOXA11, HOXA9, HOXA10**
Pattern specification process	10	1.10E−02	6.30E−01	**HOXA10, HOXA11, HOXA9, HOXC6, HOXD10, HHIP,** FOXF1, FLT1, KIF3A, SF3B1
Anterior/posterior pattern formation	7	1.20E−02	6.6OE−01	**HOXA10, HOXA11, HOXA9, HOXC6, HOXD10,** KIF3A, SF3B1
Regionalization	8	1.80E−02	7.20E−01	**HOXA10, HOXA11, HOXA9, HOXC6, HOXD10, HHIP,** KIF3A, SF3B1
Embryonic limb morphogenesis	4	1.10E−01	8.60E−01	**HOXA10, HOXA11, HOXA09, HOXC6, HOXD10**
Embryonic appendage morphogenesis	4	1.10E−01	8.60E−01	**HOXA10, HOXA11, HOXA09, HOXC6, HOXD10**
Embryonic morphogenesis	8	1.20E−01	8.70E−01	**HOXA10, HOXA11, HOXA9, HOXA10,** FOXF1, CLF1, GRLF1, PPAP2B
Skeletal system development	8	1.40E−01	8.80E−01	**HOXA10, HOXA11, HOXA9, HOXD10, COL1A1,** CLEC3B, WWOX
Limb morphogenesis	4	1.50E−01	8.90E−01	**HOXA10, HOXA11, HOXA9, HOXD10**
Appendage morphogenesis	4	1.50E−01	8.90E−01	**HOXA10, HOXA11, HOXA9, HOXD10**
Appendage development	4	1.60E−01	8.90E−01	**HOXA10, HOXA11, HOXA9, HOXD10**
Limb development	4	1.60E−01	8.90E−01	**HOXA10, HOXA11, HOXA9, HOXD10**
Sequence-specific DNA binding	10	4.10E−01	9.60E−01	**HOXA10, HOXA11, HOXA9, HOXD10, FOS,** FOXF1, HSPD1, HNRNPA2B1, MAFK
B				
Regulation of gene expression, epigenetic	6	3.90E−03	4.60E−01	*ARID1A, DNMT1, ATF7IP, EIF2C1, HELLS,* **FOS**
DNA methylation	4	4.00E−03	4.30E−01	*DNMT1, ATF7IP, HELLS,* **FOS**
DNA alkylation	4	4.00E−03	4.30E−01	*DNMT1, ATF7IP, HELLS,* **FOS**
DNA modification	4	9.90E−03	6.30E−01	*DNMT1, ATF7IP, HELLS,* **FOS**
One-carbon metabolic process	5	6.50E−02	8.30E−01	*DNMT1, ATF7IP, HELLS,* **FOS,** *SHMT2*
Biopolymer methylation	4	6.70E−02	8.20E−01	*DNMT1, ATF7IP, HELLS,* **FOS**
Methylation	4	8.40E−02	8.30E−01	*DNMT1, ATF7IP, HELLS,* **FOS**
Negative regulation of transcription	8	4.30E−01	9.70E−01	*DNMT1, ATF7IP, HELLS, SUM01, SMARCE1, AKIRIN2, GRLF1, ZFP161*
Negative regulation of transcription, DNA-dependent	5	7.10E−01	1.00E + 00	*DNMT1, ATF7IP, HELLS, SMARCE1, ZFP161*
Negative regulation of RNA metabolic process	5	7.30E−01	1.00E + 00	*DNMT1, ATF7IP, HELLS, SMARCE1, ZFP161*
Negative regulation of transcription from RNA polymerase II promoter	3	8.80E−01	1.00 + 00	*DNMT1, ATF7IP, ZFP161*

pattern formation, nucleotide binding, DNA replication, stress response, transcription regulation, ubiquitination, cell cycle and common cellular processes (data not shown). We further focussed on the clusters displayed in Table 1A and B. All terms listed in Table 1A have a strong association to the expression of *HOX* genes which are mainly responsible for pattern formation, skeletal development and embryonic morphogenesis. Most prominent genes within this cluster were among others the *FBJ murine osteosarcoma viral oncogene homolog*; *FOS* which is a transcription factor playing a role in bone development (Grigoriadis et al., 1995), the *hedgehog-interacting protein; HHIP* belonging to the hedgehog (Hh) gene family encoding signaling molecules that are involved in regulating morphogenesis and *collagen, typeI, alpha-1*; *COL1A1* one of the most prominent collagens of bone and important target gene in treatment of osteogenesis imperfecta (Chamberlain et al., 2004). These three genes were regarded as potential candidate genes relevant in the modulation of USSCs initialized by co-culture and therefore validated by qPCR (Fig. 6). *COL1A1* was upregulated in 2 out of 3 cases. However, USSC1 revealed a strong *COL1A1* expression already at day 0 which was downregulated after 5 days of co-culture with CDSC1. The expression level in all USSC samples compared to the CDSC line was already higher at day 0 compared to CDSC d0 and tended to increase during co-culture. The expression of *HHIP* was higher as well in USSCs at day 0 but strongly increased in all samples after 16 h of co-culture. However, after 5 days of co-culture the expression of *HHIP* decreased and reached an even lower level as compared to native USSCs. Moreover, *HHIP* appeared to be adjusted to the expression

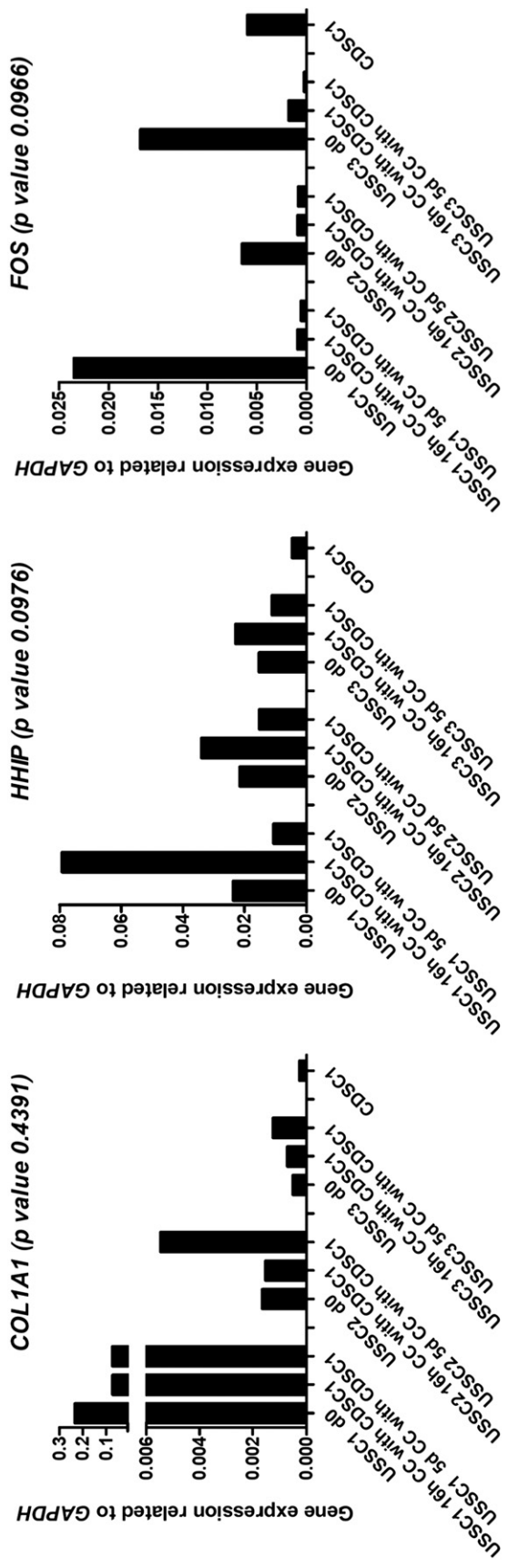

Fig. 6 Differentially expressed candidate genes *COL1A1*, *HHIP* and *FOS* were validated by qPCR: USSC lines (n = 3) were co-cultivated for 16 h (16 h) and for 5 days (5d) with CDSC1 and then analysed directly for the markers *COL1A1*, *HHIP* and *FOS* in comparison to the parental cell line without co-culture (d0). The gene expression is normalized in relation to *GAPDH*.

level of the co-cultivated CDSC line. Regarding the expression of *FOS*, the very strong downregulation (Fold changes: USSC1 −46,48; USSC2 -8.13, USSC3 -80.44) was observed in all USSC lines tested in accordance with the Affymetrix microarrays (see Supplementary Table 2), fold change: -12.22). Notably, *FOS* is one of the prominent genes associated to the GO terms annotated to epigenetic regulations (Table 1B). Taken together, the microarray data confirmed our former results and helped to find additional potential candidate genes involved in the cell fate switch of USSCs after co-culture.

Discussion

Although stromal cell populations can be isolated from numerous human tissues (Fraser et al., 2006; Griffiths et al., 2005; Kogler et al., 2009), their developmental origins remain largely unknown and their characterization is discussed controversially (Bianco, 2011a; Bianco, 2011b). USSCs display a strong similarity to CDSCs and BMSCs in their immunophenotype and their osteogenic and chondrogenic differentiation potential *in vitro*, but differ in their restricted adipogenic potential (Kluth et al., 2010). In 2010, we were able to distinguish these two functionally distinct neonatal stromal cell populations derived from cord blood additionally on the *HOX* gene expression pattern (Liedtke et al., 2010). In order to define if the limited adipogenic differentiation potential in USSCs is reflected by the *HOX* gene expression, co-culture experiments were performed. The hypothesis was pursued that co-culture of USSCs (HOX^-) with CDSCs and BMSCs (HOX^+) could be sufficient to adapt the *HOX* expression pattern of a surrounding cell as it was shown before in mice for periosteal progenitor cells (Leucht et al., 2008). For the first time, the results of our study clearly demonstrate in detail that adaption of the *HOX* code by co-culture is possible in the human system for CB-derived subpopulations. Notably, the adaption of the *HOX* code attends with a cell fate switch of USSCs gaining an adipogenic differentiation potential. These results imply that the adaptiveness of USSCs to surrounding cells is an important feature when using these cells in therapeutical approaches. In addition the impact of the co-culture on the osteogenic differentiation capacity was tested. Both USSC and CDSC lines can be easily differentiated towards the chondrogenic and osteogenic lineage but can individually differ in the content of proteoglycans in chondrogenesis or in the level of mineralization during osteogenesis. Co-cultured USSCs revealed an adaption to the CDSC line reflected by a lower level of proteoglycans detected at day 21 of chondrogenic differentiation. Co-culture of a CDSCs with lower mineralization than USSCs revealed an adjustment of the USSCs to the mineralization level of the CDSCs. Furthermore, these results were confirmed on transcript level for several osteo/chondro-associated genes.

Co-culture of CDSCs with USSCs revealed regulation of osteo- and chondro-associated markers, from which *BMP2*, *BMP4*, *PTHLH*, *ACAN* and *FOXF1* were upregulated and *BSP*, *RUNX2*, *SOX9*, *TWIST1* and *MSX2* were downregulated after co-culture (Supplementary Fig. 8). Many different transcription factors and regulatory signals are involved in the endochondral ossification. The runt domain-containing transcription factor 2 (RUNX2) is necessary for osteoblast differentiation and the correct function of mature osteoblasts. Furthermore, RUNX2 plays an important role in chondrocyte maturation (Adams et al., 2007; Long, 2012). Downstream of RUNX2, the Sp7 transcription factor (OSX) is essential for the embryonic as well as the postnatal osteoblast and osteocyte differentiation and function (Long, 2012). A negative regulator strongly involved in endochondral ossification is the parathyroid hormone-related protein (PTHLH). This protein promotes chondrocyte proliferation and delays the differentiation, ensuring a supply of proliferating chondrocytes needed for skeletal growth. Expression of PTHLH negatively regulates RUNX2, which is required for the chondrocyte maturation (Adams et al., 2007). All of the transcription factors are regulated by a variety of developmental signals, including Hedgehog proteins, Notch signaling, Wnt signaling, BMP signaling and FGF signaling (Long, 2012) confirmed by our data. BMP2 is known to be upregulated during osteogenesis as well as during adipogenesis (Ahrens et al., 1993) and we were able to confirm this. MSX2 promotes osteoblast differentiation independently of Runx2 and negatively regulates adipocyte differentiation (Ichida et al., 2004). Our PCR results clearly demonstrated a downregulation of MSX2. This is in agreement with published literature (Takada et al., 2009) and may support the idea of an osteogenic to adipogenic switch in USSCs after co-culture. This hypothesis is further validated by the adapted osteogenic potential of USSCs co-cultured with a CDSC line displaying a weaker osteogenic potential. After osteogenic differentiation of co-cultured USSCs, adapted to the osteogenic potential of the CDSC line as a significantly weaker calcification level could be detected by Alizarin quantification.

Our results are further in agreement with the understanding of bone development accompanied by a temporal reactivation of *HOX* genes in a close network with TGFβ/BMP and Wnt signaling (Goldring et al., 2006).

The most downregulated gene involved in the TGFβ pathway was *FOS*. The proto-oncogene FOS has been found to be involved in the cell differentiation along the osteoclast/macrophage lineages, consequently playing a role in bone remodeling (Grigoriadis et al., 1994). Krosl et al. demonstrated that the upregulation of *HOXB4*, *HOXA9* or *HOXB3* leads to a decrease in the expression of *c-Fos* in rat cells (Krosl and Sauvageau, 2000). These results are in line with our findings that the expression of *FOS* is down-regulated after *HOX* gene expression is upregulated.

In addition to the TGFβ pathway Wnt signaling has been connected to many different developmental events during embryogenesis as well as to adult tissue homeostasis by affecting mitogenic stimulation, cell fate specification and differentiation (Logan and Nusse, 2004). Furthermore loss of Wnt signalling causes a cell fate shift of preosteoblast from osteoblasts to adipocytes (Song et al., 2012). The Affymetrix gene expression analyses performed in this study confirmed the data presented in this work. Gene ontology terms enriched for differentially expressed genes reflected the processes observed in USSCs. Beside typical cellular processes especially the bone formation and patterning associated terms substantiate our data. Most notably confirming the data presented for *HOX* genes as well as for osteo-specific genes. One of genes found to be most strongly regulated was *FOS*. Besides its critical functions in bone development, FOS is suggested to be involved in epigenetic regulations (Bakin and Curran, 1999) reflecting the GO terms displayed in Table 1B. Therefore, FOS

is supposed to be one of the most promising key players in the processes described here.

Taken together, the results presented in this work clearly demonstrate the adaptiveness of USSCs regarding their differentiation potential.

After co-culture USSCs adjust their differentiation capacities to the stromal cell lines used in the experiments. The USSCs revealed *HOX* gene expression and an adipogenic differentiation potential. As an adaption to the CDSC type could be revealed *in vitro*, a molecular switching of osteogenesis versus adipogenesis was initiated in USSCs by simple co-culture experiments.

We are convinced that the spatio-temporal regulation of *HOX* genes during fetal development can biologically reflect the adaptiveness of cells presented here. It can be hypothesized that USSCs can be regarded as developmentally earlier cell type in cord blood as compared to CDSCs. Until now no experiments were able to define the fetal origin of these cells. A negative *HOX* code of cells seems to provide a more unrestricted status of progenitor cells and this can be regarded as a mandatory feature for cells to adapt to the surrounding niche. Moreover, the positive HOX code of CDSCs seems to restrict cells in their regenerative potential, as it was shown by Leucht et al. (2008) for the HOX positive tibial progenitor cells. Therefore a speculative explanation might be that cells, already "imprinted" by their surrounding niche, loose their adaptiveness reflected by the positive HOX code. Consequently this method provides important insights into molecular regulations of this process. Moreover, USSCs can be claimed as potential candidates to substitute unique progenitor cell populations as Leucht et al. (2008) presented in mice that not every progenitor cell has a sufficient regenerative capacity leading to a complete bone repair dependent on the inherent HOX code of the cell. Transferring these results from Leucht and colleagues to our *in vitro* cell model the relevance of the inherent HOX code of a cell not only reflects the developmental origin of a cell but moreover the inherent regenerative potential of progenitor and/or stromal cells like the HOX negative USSCs. Others just recently described differential *HOX* gene expression reflecting distinct aortic cell populations (Trigueros Motos et al., 2013). Their data support our hypothesis that the inherent HOX code of a cell can moreover be linked to functional differences as described here.

As USSCs seem to be unrestricted in their *HOX* gene expression, the adaptiveness to the surrounding cells/niche seems to be an important prerequisite of a progenitor cell to adapt the regenerative potential. Further experiments will be needed to validate these new findings *in vivo* to evaluate the impact of the inherent HOX code with regard to clinical applications. However, the experiments described here clearly consolidate the necessity to better characterize stromal cells and their inherent regenerative potential when applying them in clinical approaches. We are convinced that in this context the adaptiveness of cells is higher in HOX^{-} cells as compared to HOX^{+} cells, which seem to be more restricted.

Conclusion

Our data present for the first time important insights into possible modulations of cell fate decisions in the human neonatal system initiated by direct co-culture experiments of USSCs with CDSCs and BMSCs. Furthermore, USSCs can be claimed as potential candidates to substitute unique progenitor cell populations in clinical approaches.

Acknowledgments

We would like to thank Daniela Stapelkamp for her excellent technical support and acknowledge the assistance of the Core Flow Cytometry Facility at the Institute for Transplantation Diagnostics and Cell Therapeutics Düsseldorf, especially Katharina Raba for cell sorting. In addition we would like to thank the Department of Cardiovascular Surgery (Düsseldorf), especially Andrey Fomin for providing their confocal microscopy expertise. The contribution of Julia Bosch was supported by the Jürgen Manchot Stiftung. The work was supported by the Deutsche Forschungsgemeinschaft (DFG) grant Ko2119/8-1.

Appendix A. Supplementary data

Supplementary data to this article can be found online at http://dx.doi.org/10.1016/j.scr.2013.04.001.

References

Abdallah, B.M., Kassem, M., 2009. The use of mesenchymal (skeletal) stem cells for treatment of degenerative diseases: current status and future perspectives. J. Cell. Physiol. 218, 9–12.

Adams, S.L., Cohen, A.J., Lassova, L., 2007. Integration of signaling pathways regulating chondrocyte differentiation during endochondral bone formation. J. Cell. Physiol. 213, 635–641.

Ahrens, M., Ankenbauer, T., Schroder, D., Hollnagel, A., Mayer, H., Gross, G., 1993. Expression of human bone morphogenetic proteins-2 or −4 in murine mesenchymal progenitor C3H10T1/2 cells induces differentiation into distinct mesenchymal cell lineages. DNA Cell Biol. 12, 871–880.

Bakin, A.V., Curran, T., 1999. Role of DNA 5-methylcytosine transferase in cell transformation by fos. Science 283, 387–390.

Bianco, P., 2011a. Back to the future: moving beyond "mesenchymal stem cells". J. Cell. Biochem. 112, 1713–1721.

Bianco, P., 2011b. Minireview: the stem cell next door: skeletal and hematopoietic stem cell "niches" in bone. Endocrinology 152, 2957–2962.

Bolstad, B.M., Irizarry, R.A., Astrand, M., Speed, T.P., 2003. A comparison of normalization methods for high density oligonucleotide array data based on variance and bias. Bioinformatics 19, 185–193.

Bosch, J., Houben, A.P., Radke, T.F., Stapelkamp, D., Bunemann, E., Balan, P., Buchheiser, A., Liedtke, S., Kogler, G., 2012. Distinct differentiation potential of "MSC" derived from cord blood and umbilical cord: are cord-derived cells true mesenchymal stromal cells? Stem Cells Dev. 21, 1977–1988.

Chamberlain, J.R., Schwarze, U., Wang, P.R., Hirata, R.K., Hankenson, K.D., Pace, J.M., Underwood, R.A., Song, K.M., Sussman, M., Byers, P.H., Russell, D.W., 2004. Gene targeting in stem cells from individuals with osteogenesis imperfecta. Science 303, 1198–1201.

Creuzet, S., Couly, G., Vincent, C., Le Douarin, N.M., 2002. Negative effect of Hox gene expression on the development of the neural crest-derived facial skeleton. Development 129, 4301–4313.

Dennis Jr., G., Sherman, B.T., Hosack, D.A., Yang, J., Gao, W., Lane, H.C., Lempicki, R.A., 2003. DAVID: Database for Annotation, Visualization, and Integrated Discovery. Genome Biol. 4, 3.

Dominici, M., Le Blanc, K., Mueller, I., Slaper-Cortenbach, I., Marini, F., Krause, D., Deans, R., Keating, A., Prockop, Dj, Horwitz, E., 2006. Minimal criteria for defining multipotent

mesenchymal stromal cells. The International Society for Cellular Therapy position statement. Cytotherapy 8, 315–317.

Erices, A., Conget, P., Rojas, C., Minguell, J.J., 2002. Gp130 activation by soluble interleukin-6 receptor/interleukin-6 enhances osteoblastic differentiation of human bone marrow-derived mesenchymal stem cells. Exp. Cell Res. 280, 24–32.

Fraser, J.K., Wulur, I., Alfonso, Z., Hedrick, M.H., 2006. Fat tissue: an underappreciated source of stem cells for biotechnology. Trends Biotechnol. 24, 150–154.

Goldring, M.B., Tsuchimochi, K., Ijiri, K., 2006. The control of chondrogenesis. J. Cell. Biochem. 97, 33–44.

Griffiths, M.J., Bonnet, D., Janes, S.M., 2005. Stem cells of the alveolar epithelium. Lancet 366, 249–260.

Grigoriadis, A.E., Wang, Z.Q., Cecchini, M.G., Hofstetter, W., Felix, R., Fleisch, H.A., Wagner, E.F., 1994. c-Fos: a key regulator of osteoclast-macrophage lineage determination and bone remodeling. Science 266, 443–448.

Grigoriadis, A.E., Wang, Z.Q., Wagner, E.F., 1995. Fos and bone cell development: lessons from a nuclear oncogene. Trends Genet. 11, 436–441.

Gruss, P., Kessel, M., 1991. Axial specification in higher vertebrates. Curr. Opin. Genet. Dev. 1, 204–210.

Hansen, S.L., Myers, C.A., Charboneau, A., Young, D.M., Boudreau, N., 2003. HoxD3 accelerates wound healing in diabetic mice. Am. J. Pathol. 163, 2421–2431.

Huang da, W., Sherman, B.T., Lempicki, R.A., 2009. Systematic and integrative analysis of large gene lists using DAVID bioinformatics resources. Nat. Protoc. 4, 44–57.

Ichida, F., Nishimura, R., Hata, K., Matsubara, T., Ikeda, F., Hisada, K., Yatani, H., Cao, X., Komori, T., Yamaguchi, A., Yoneda, T., 2004. Reciprocal roles of MSX2 in regulation of osteoblast and adipocyte differentiation. J. Biol. Chem. 279, 34015–34022.

Jeltsch, K.S., Radke, T.F., Laufs, S., Giordano, F.A., Allgayer, H., Wenz, F., Zeller, W.J., Kogler, G., Fruehauf, S., Maier, P., 2011. Unrestricted somatic stem cells: interaction with CD34+ cells *in vitro* and *in vivo*, expression of homing genes and exclusion of tumorigenic potential. Cytotherapy 13, 357–365.

Kluth, S.M., Buchheiser, A., Houben, A.P., Geyh, S., Krenz, T., Radke, T.F., Wiek, C., Hanenberg, H., Reinecke, P., Wernet, P., Kogler, G., 2010. DLK-1 as a marker to distinguish unrestricted somatic stem cells and mesenchymal stromal cells in cord blood. Stem Cells Dev. 19, 1471–1483.

Kmita, M., Duboule, D., 2003. Organizing axes in time and space; 25 years of colinear tinkering. Science 301, 331–333.

Kogler, G., Sensken, S., Airey, J.A., Trapp, T., Muschen, M., Feldhahn, N., Liedtke, S., Sorg, R.V., Fischer, J., Rosenbaum, C., Greschat, S., Knipper, A., Bender, J., Degistirici, O., Gao, J., Caplan, A.I., Colletti, E.J., Almeida-Porada, G., Muller, H.W., Zanjani, E., Wernet, P., 2004. A new human somatic stem cell from placental cord blood with intrinsic pluripotent differentiation potential. J. Exp. Med. 200, 123–135.

Kogler, G., Radke, T.F., Lefort, A., Sensken, S., Fischer, J., Sorg, R.V., Wernet, P., 2005. Cytokine production and hematopoiesis supporting activity of cord blood-derived unrestricted somatic stem cells. Exp. Hematol. 33, 573–583.

Kogler, G., Critser, P., Trapp, T., Yoder, M., 2009. Future of cord blood for non-oncology uses. Bone Marrow Transplant. 44, 683–697.

Krosl, J., Sauvageau, G., 2000. AP-1 complex is effector of Hox-induced cellular proliferation and transformation. Oncogene 19, 5134–5141.

Krumlauf, R., 1994. Hox genes in vertebrate development. Cell 78, 191–201.

Leucht, P., Kim, J.B., Amasha, R., James, A.W., Girod, S., Helms, J.A., 2008. Embryonic origin and Hox status determine progenitor cell fate during adult bone regeneration. Development 135, 2845–2854.

Liedtke, S., Buchheiser, A., Bosch, J., Bosse, F., Kruse, F., Zhao, X., Santourlidis, S., Kogler, G., 2010. The HOX Code as a "biological fingerprint" to distinguish functionally distinct stem cell populations derived from cord blood. Stem Cell Res. 5, 40–50.

Logan, C.Y., Nusse, R., 2004. The Wnt signaling pathway in development and disease. Annu. Rev. Cell Dev. Biol. 20, 781–810.

Lohberger, B., Payer, M., Rinner, B., Kaltenegger, H., Wolf, E., Schallmoser, K., Strunk, D., Rohde, E., Berghold, A., Pekovits, K., Wildburger, A., Leithner, A., Windhager, R., Jakse, N., 2012. Tri-lineage potential of intraoral tissue-derived mesenchymal stromal cells. J. Craniomaxillofac. Surg. 41, 110–118.

Long, F., 2012. Building strong bones: molecular regulation of the osteoblast lineage. Nat. Rev. Mol. Cell Biol. 13, 27–38.

Sherman, B.T., Huang da, W., Tan, Q., Guo, Y., Bour, S., Liu, D., Stephens, R., Baseler, M.W., Lane, H.C., Lempicki, R.A., 2007. DAVID Knowledgebase: a gene-centered database integrating heterogeneous gene annotation resources to facilitate high-throughput gene functional analysis. BMC Bioinforma. 8, 426.

Song, L., Liu, M., Ono, N., Bringhurst, F.R., Kronenberg, H.M., Guo, J., 2012. Loss of wnt/beta-catenin signaling causes cell fate shift of preosteoblasts from osteoblasts to adipocytes. J. Bone Miner. Res. 27, 2344–2358.

Takada, I., Kouzmenko, A.P., Kato, S., 2009. Molecular switching of osteoblastogenesis versus adipogenesis: implications for targeted therapies. Expert Opin. Ther. Targets 13, 593–603.

Trigueros Motos, L., Gonzalez Granado, J.M., Cheung, C., Fernandez, P., Sanchez Cabo, F., Dopazo, A., Sinha, S., Andres, V., 2013. Embryological-origin-dependent differences in Hox expression in adult aorta: role in regional phenotypic variability and regulation of NF-κB activity. Arterioscler. Thromb. Vasc. Biol. 33 (Epub ahead of print).

Supplementary data

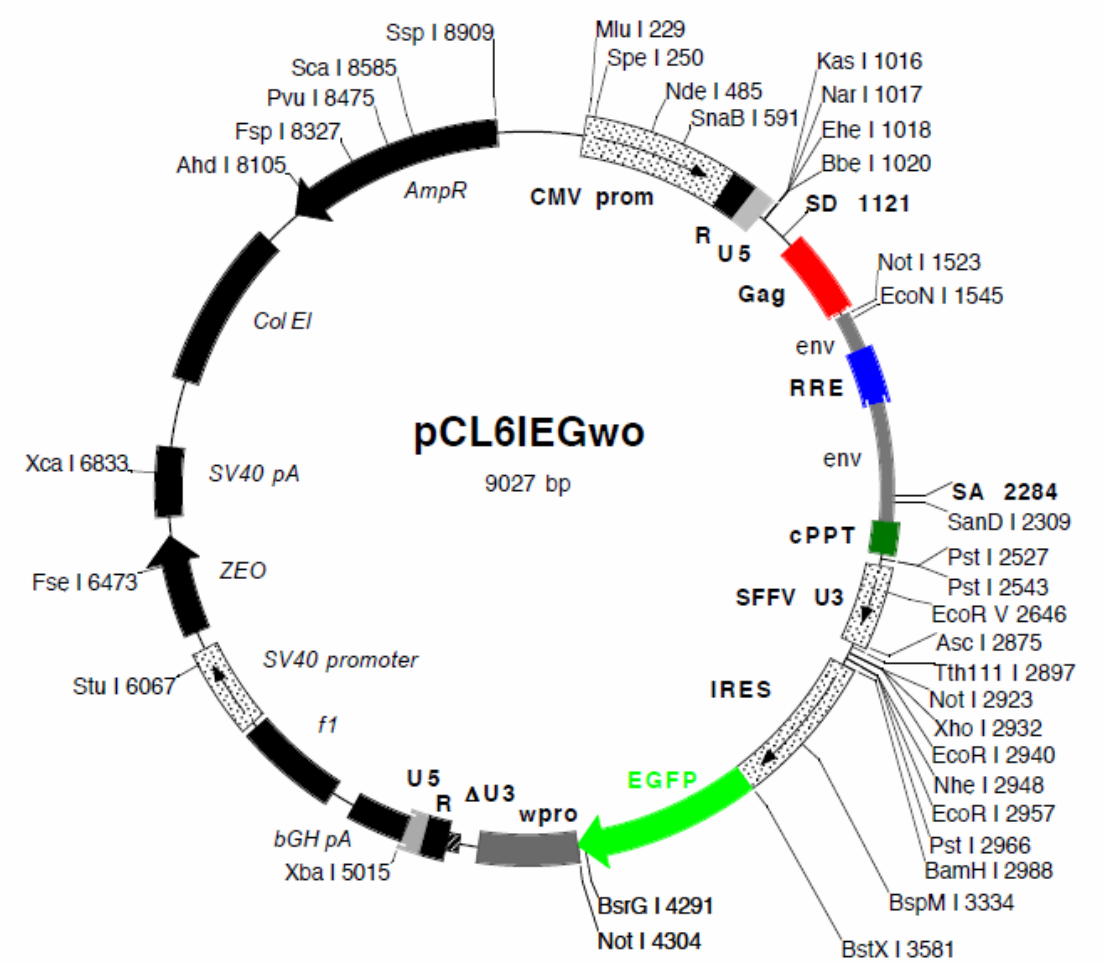

The following enzymes do not cut in pCL6IEGwo:

Age I	Blp I	BsaB I	BsiW I	BsmB I
BspE I	BstB I	BstE II	Bsu36 I	Cla I
Eco47 III	Esp I	Hpa I	Pac I	Pme I
Rsr II	Sfi I	Spl I	Srf I	Swa I
Xcm I				

Plasmid name: pCL6 IEGwo
Plasmid size: 9027 bp
Constructed by: Constanze Wiek
Construction date: 6'2007
Comments: Cut the WPRO element with BsrG I-Not I out of puc2MD9 EF1a WPRO and cloned into pCL6IEG cut bsmB I, blunded with Klenow and then cut BsrG I. IRES 2993-3580. EGFP 3581-4300 (720). WPRO 4307-4708. Corrected according to sequencing 4708del11

Supplementary Fig. 1: Plasmid card of the GFP containing vector pCL6IEGwo.

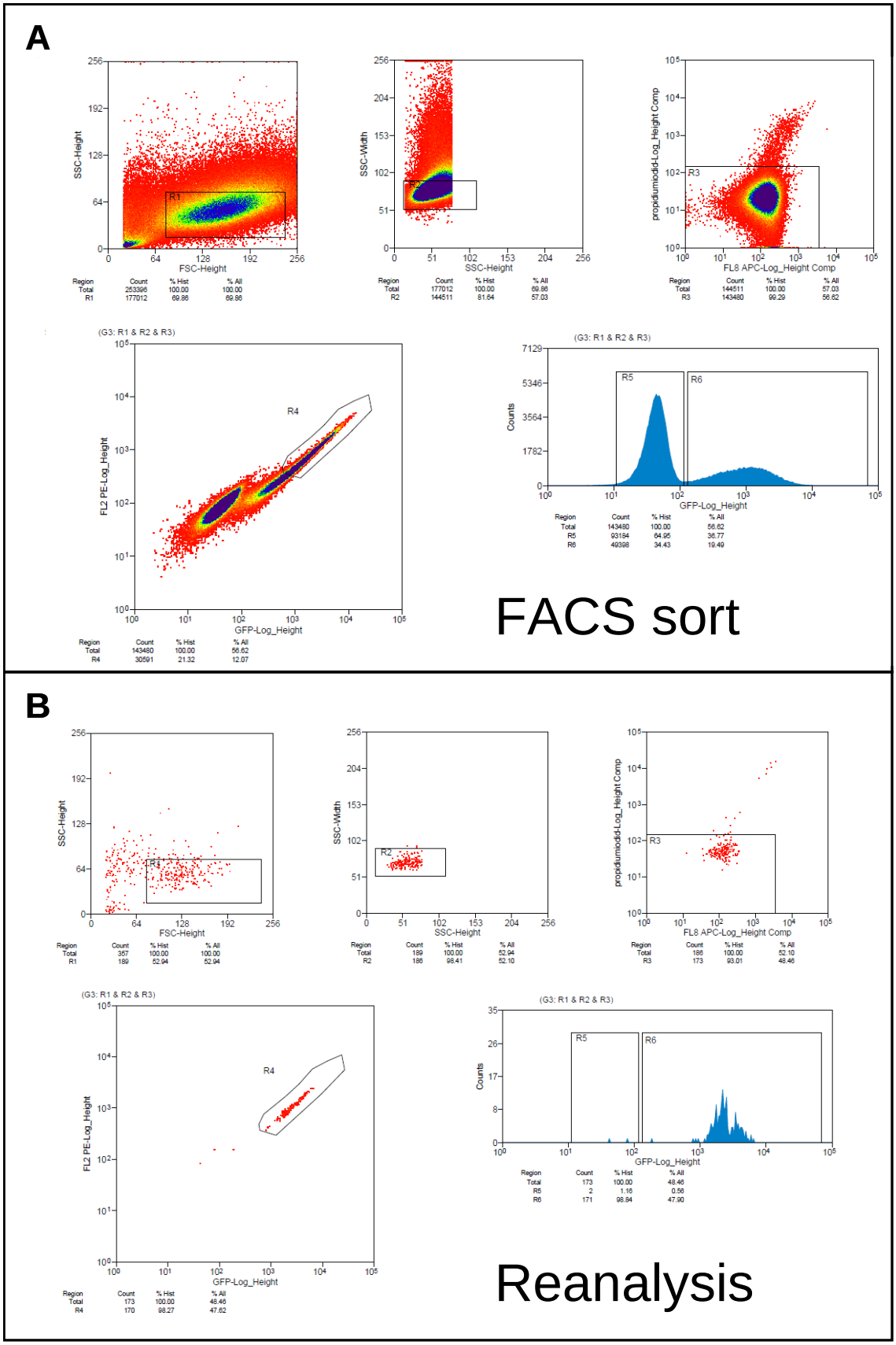

Supplementary Fig. 2: Stringency of FACS sorting strategy. A: In these dot plots the applied sorting gate R4 is depicted. Only 10% of the highly GFP-expressing cells were sorted. **B:** Reanalysis of cells revealed 1,7% of cells without GFP fluorescence.

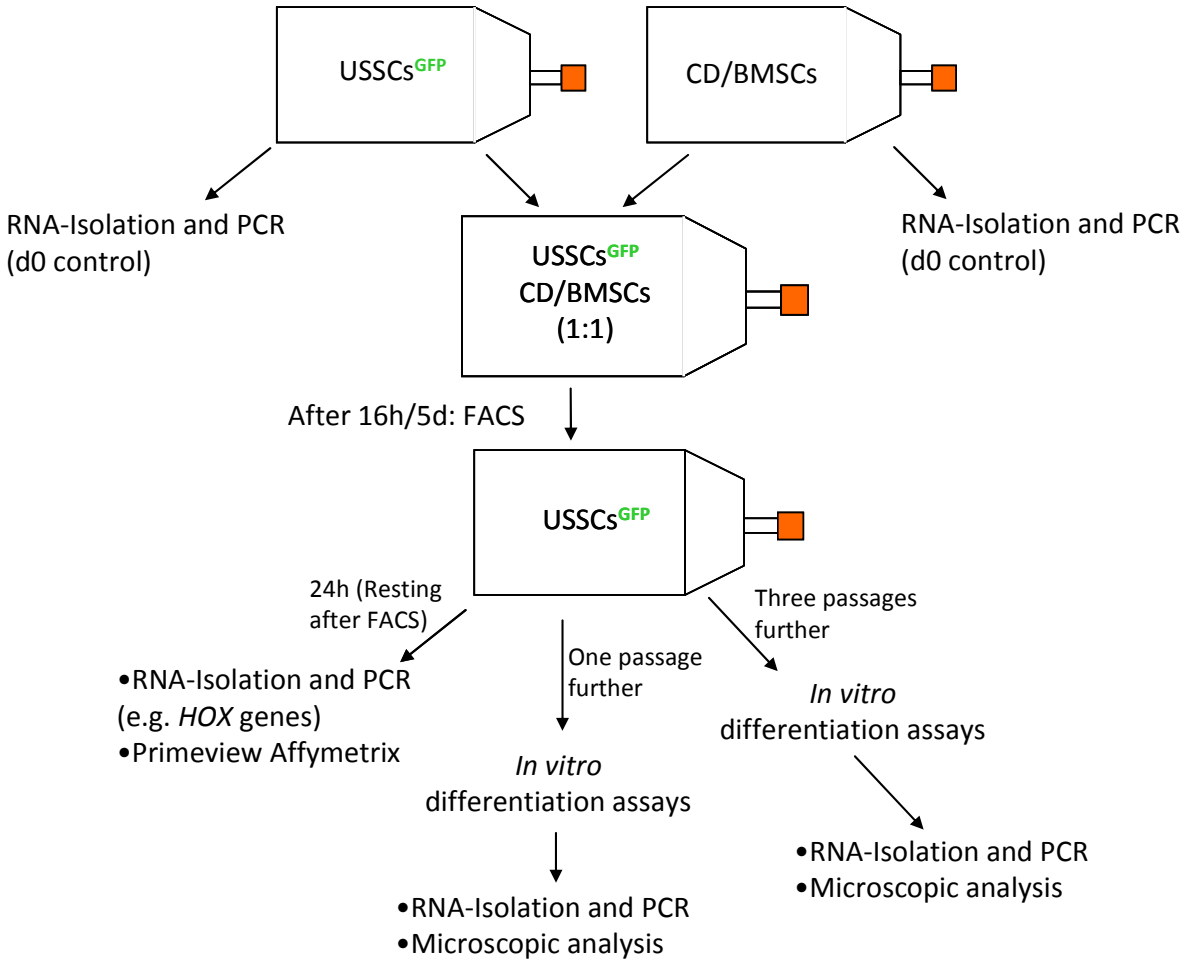

Supplementary Fig. 3: Schematic procedure of co-culture experiments and subsequent analyses.

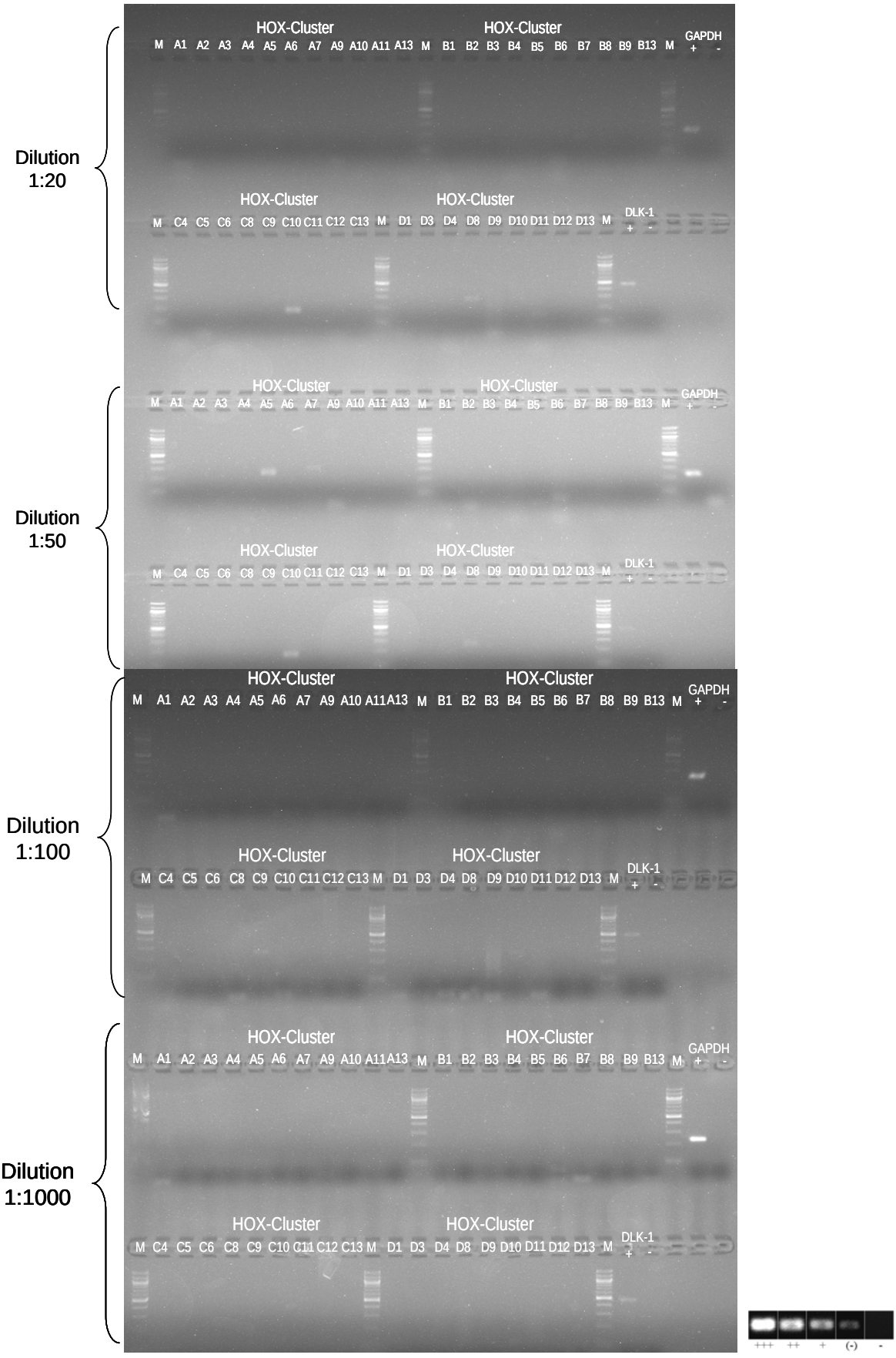

Supplementary Fig. 4: Dilution experiments of CDSCs with USSCs. Agarosegel pictures of resulting PCR products are depicted. Rare weak bands for *HOXA5*, *HOXC10* and *HOXD8* were detectable in the 1:20 and 1:50 dilution. In following co-culture experiments only bands above this band intensity were judged “positive” (see legend). Dilutions were prepared as followed: Freshly trypsinized USSCs and CDSCs were counted using a Cell-Dyn (Abbott Diagnostics) and then mixed in the dilutions mentioned above. The RNA was isolated subsequently.

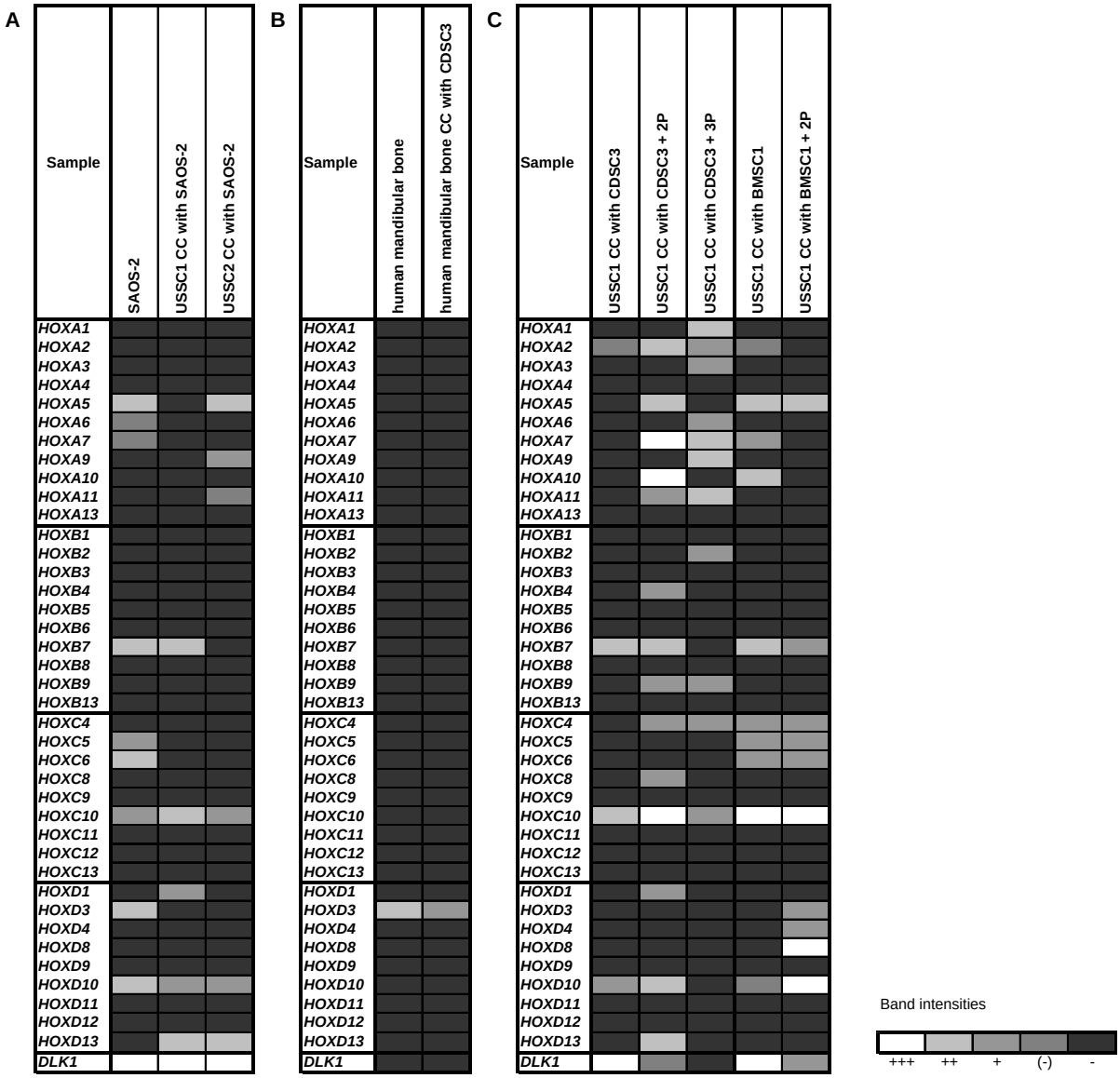

Supplementary Fig. 5: A: USSCs reveal *HOX* gene expression after co-culture with SAOS-2 cells. USSCs co-cultivated for 5 days with SAOS-2 (osteosarcoma cell line) cells were sorted by FACS and subsequently tested for expression of 39 *HOX* genes and adipogenesis inhibitor *DLK1* by RT PCR. **B: *HOX*- human mandibular bone cells remain *HOX* negative after co-culture with CDSCs.** *HOX*- human mandibular bone cells were co-cultivated for 5 days with a CDSC line, sorted by FACS and subsequently tested for expression of 39 *HOX* genes and adipogenesis inhibitor *DLK1* by RT PCR. **C: *HOX* gene expression of co-cultivated USSCs is accumulating after subsequent passaging.** USSCs co-cultivated for 5 days with either CDSCs or BMSCs were sorted by FACS, further cultivated for up to 3 subsequent passages (+2P, +3P) and finally tested for the expression of 39 *HOX* genes and adipogenesis inhibitor *DLK1* by RT PCR. Intensity of product bands was judged from negative "–" to strongly positive "+++" in a graduated manner (for examples see legend) and visualized by a heat map.

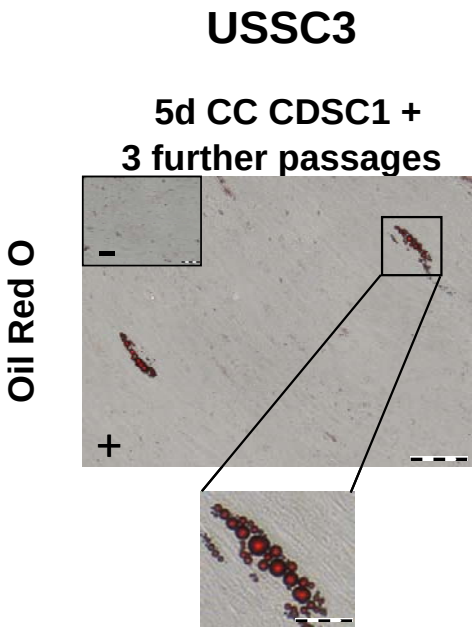

Supplementary Fig. 6: USSCs keep the adipogenic differentiation potential after five days of co-culture with CDSCs and further 3 passages. USSC3 were co-cultured (CC) for 5 days with CDSC1. After FACS sort cells were cultivated for 1 further passage and then differentiated into the adipogenic direction for 21 days (d21). After adipogenic differentiation cells were cultivated without induction medium for 3 further passages and adipogenic differentiation potential was visualized by Oil-red-O staining. Exemplified light microscopic photographs of cells stained with Oil-red-O (detects neutral triglycerides and lipids) after three passages adipogenic differentiation in differentiated (+) and control cells (-). Scale bar: 100µm and 25µm in the enlarged images.

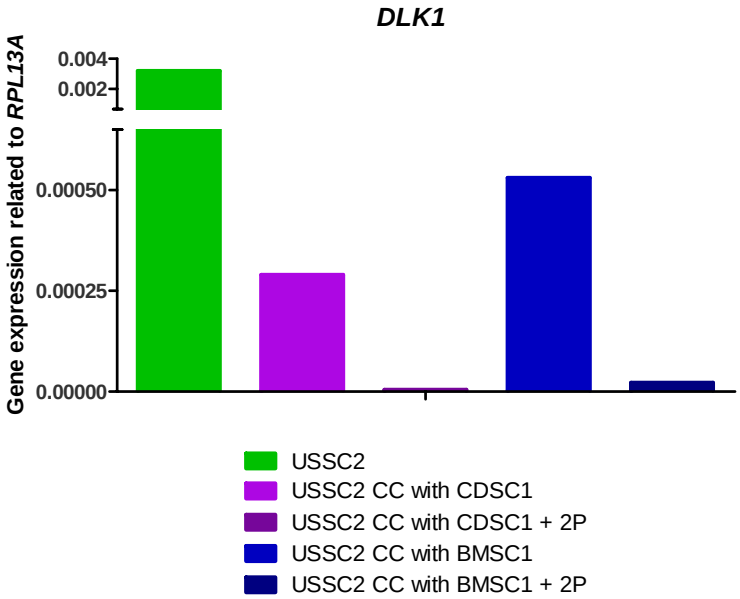

Supplementary Fig. 7: The adipogenic inhibitor *DLK1* is downregulated in co-cultivated USSCs after 2 passages. USSCs2 was co-cultivated with CDSCs1 and BMSCs1 and then analyzed directly and after two further passages (+2P) for the adipogenic inhibitor *DLK1* in comparison to the parental cell line without co-culture. The gene expression is illustrated in relation to *RPL13A*.

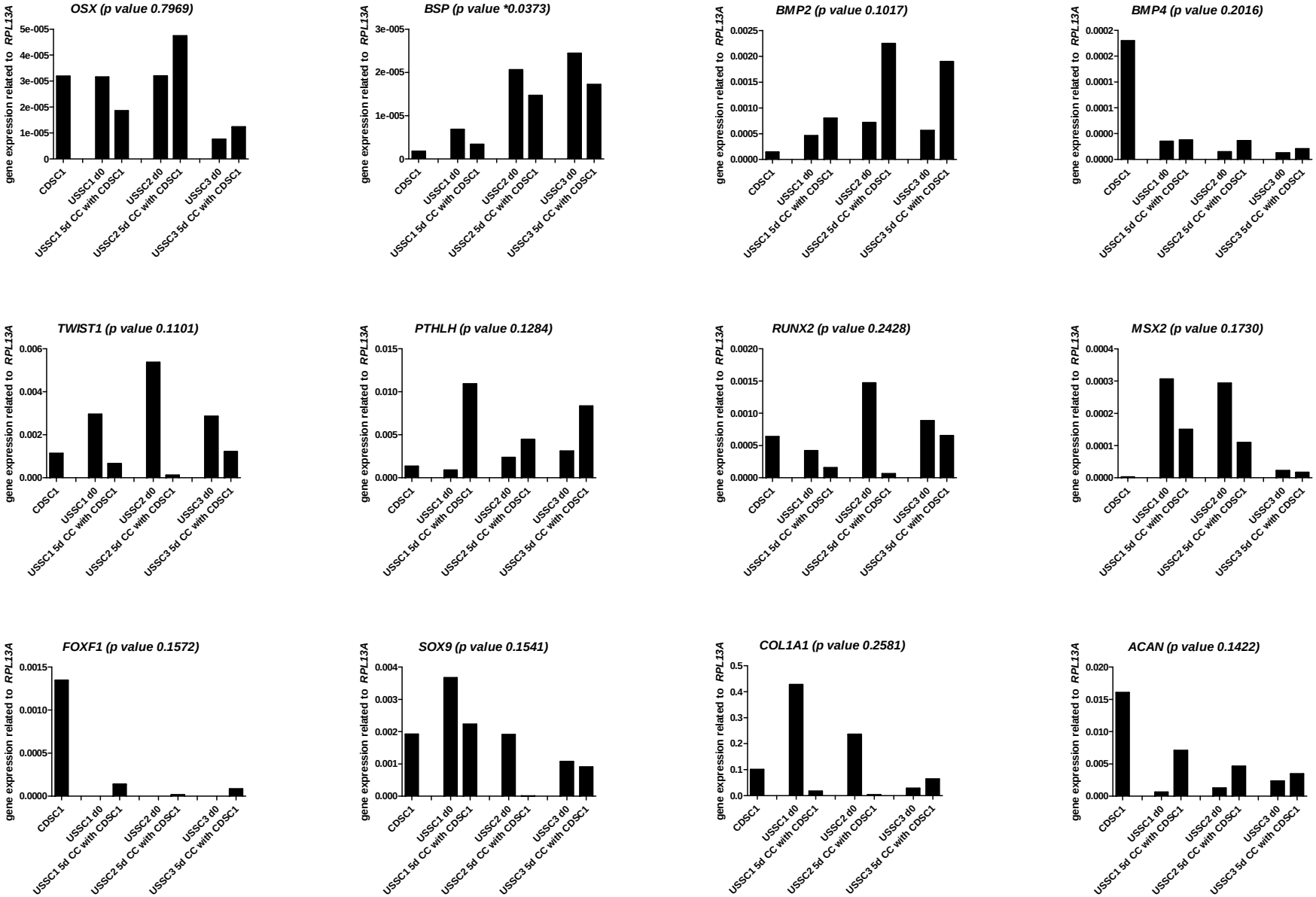

Supplementary Fig. 8: Osteogenic markers were regulated in USSCs after co-culture. USSC lines (n=3) were co-cultivated (CC) for 5 days with CDSC1 and analyzed directly for the osteogenic markers *OSX, BSP, BMP2, BMP4,* osteo/chondro-associated genes *TWIST1*, *PTHLH*, *RUNX2, MSX2*, *FOXF1* and chondro-related genes *SOX9*, *COL1A1* and *ACAN* in comparison to the parental cell line without co-culture. A paired t-test was applied to detect significant regulation. Respective p-values are given in the head line with the gene name.

Supplementary Tab. 1: Primer sequences. The gene expression analyses were performed by quantitative (real-time) PCR (qPCR). The Applied Biosystems SYBR®Green Mastermix kit, containing fluorescence dye SYBR®Green, was used for the gene-quantification. The *SOX9* expression was measured using the Applied Biosystems TaqMan® Gene Expression Assays together with TaqMan® 2xUniversal PCR Mastermix No Amp Erase® UNG according to the instructions of the manufacturer.

Gene	representative public ID	forward (5´-3´)	reverse (5´-3´)	bp	TM (°C)
ADIPOQ	NM_004797.2	TGTTGCTGGGAGCTGTTCTACTG	ATGTCTCCCTTAGGACCAATAAG	235	60
ACAN	NM_001135.3	CCAGTGCACAGAGGGGTTTG	TCCGAGGGTGCCGTGAG	146	60
BMP2	NM_001200.2	TGCGCCAGGTCCTTTGACC	AACGCTAGAAGACAGCGGGTCC	134	60
BMP4	NM_130851.2, NM_130850.2, NM_001202.3	CCACCACGAAGAACATCTGG	ACCTCGTTCTCAGGGATGC	96	60
BSP	NM_004967.3	GGGCAGTAGTGACTCATCCG	AAGCTGGATTGCAGCTAACCC	214	60
COL1A1	NM_000088.3	TGTTCAGCTTTGTGGACCTCCG	ACACCTTGCCGTTGTCGCAGA	204	60
DLK1	NM_003836.4	ACGGGGAGCTCTGTGATAGA	GCTTGCACAGACACTCGTAG	468	60
FOS	NM_005252.3	CTTACTACCACTCACCCGCAG	GTGGGAATGAAGTTGGCACTG	106	60
FOXF1	NM_001451.2	CAGCCTCTCCACGCACTC	CCTTTCGGTCACACATGCT	122	60
GAPDH	NM_002046	GAGTCAACGGATTTGGTCGT	TTGATTTTGGAGGGATCTCG	238	60
HHIP	NM_022475.1	AGTCCTGTGACAAAGCAGTG	TTCCATTGTGAGTCTGGGTC	163	60
MSX2	NM_002449.4	AATTCAGAAGATGGAGCGGCGTG	CGAGGAGCTGGGATGTGGTAAAG	145	65
OSX (SP7)	NM_001173467.1, NM_152860.1	TGCTTGAGGAGGAAGTTCAC	CTGAAAGGTCACTGCCCAC	153	60
PTHLH	NM_002820.2, NM_198966.1, NM_198965.1, NM_198964.1	GTGTTCCTGCTGAGCTACGC	GCTGTGTGGATTTCTGCGATCA	173	60
RPL13A	NM_012423.2	GAGGTATGCTGCCCCACAAA	TTCAGACGCACGACCTTGAG	136	60
RUNX2	NM_001015051.3, NM_001024630.3, NM_004348.3	GAGTGGACGAGGCAAGAG	GGACACCTACTCTCATACTG	215	60
TWIST1	NM_000474.3	GACCTAGATGTCATTGTTTCC	GCCCTGTTTCTTTGAATTTG	140	55

Supplementary Tab. 2: 278 significantly differentially expressed genes between native USSCs d0 as compared to USSCs co-cultivated with CDSCs for 5d. The absolute fold change is displayed; downregulated genes are depicted in red and upregulated genes in green.

Probe Set ID	Gene Symbol	Gene Title	Fold change (do vs d5)
11749852_s_at	FOS	FBJ murine osteosarcoma viral oncogene homolog	12.22
11734658_s_at	FOS	FBJ murine osteosarcoma viral oncogene homolog	7.03
11759131_at	HIST1H2AG	histone cluster 1, H2ag	3.35
11759804_x_at	PDCD6	programmed cell death 6	3.22
11759803_a_at	PDCD6	programmed cell death 6	3.12
11763888_at	SNORA33	small nucleolar RNA, H/ACA box 33	2.99
11758842_at	THBS1	thrombospondin 1	2.80
11758864_at	SRP19	signal recognition particle 19kDa	2.77
11740838_a_at	FAM98B	family with sequence similarity 98, member B	2.44
11727655_s_at	DST	dystonin	2.42
11762388_at	ZNF280D	zinc finger protein 280D	2.40
11715294_s_at	HECTD2	HECT domain containing 2	2.00
11760780_at	ZAK	sterile alpha motif and leucine zipper containing kinase AZK	1.97
11722690_at	SPTBN1	spectrin, beta, non-erythrocytic 1	1.93
11761728_a_at	SMARCE1	SWI/SNF related, matrix associated, actin dependent regulator of chromatin, subfamily e, member 1	1.85
11728705_at	COPG2	coatomer protein complex, subunit gamma 2	1.80
11721956_at	RFX7	regulatory factor X, 7	1.79
11756887_a_at	TENC1	tensin like C1 domain containing phosphatase (tensin 2)	1.78
11730623_at	DSEL	dermatan sulfate epimerase-like	1.74
11726965_a_at	L3MBTL3	l(3)mbt-like 3 (Drosophila)	1.74
11722752_a_at	C14orf43	chromosome 14 open reading frame 43	1.74
11744049_at	MAP1B	microtubule-associated protein 1B	1.71
11719365_x_at	SPATS2L	spermatogenesis associated, serine-rich 2-like	1.71
11725331_a_at	USP9X	ubiquitin specific peptidase 9, X-linked	1.70
11763188_a_at	SNX5	sorting nexin 5	1.69
11757956_s_at	PRTFDC1	phosphoribosyl transferase domain containing 1	1.69
11736364_s_at	KIAA0586	KIAA0586	1.68
11736086_a_at	HHIP	hedgehog interacting protein	1.68
11723798_a_at	CSTF3	cleavage stimulation factor, 3' pre-RNA, subunit 3, 77kDa	1.66
11747220_a_at	COPG2	coatomer protein complex, subunit gamma 2	1.66
11717240_at	RBBP4	retinoblastoma binding protein 4	1.66
11754984_s_at	MYH10	myosin, heavy chain 10, non-muscle	1.66
11723799_x_at	CSTF3	cleavage stimulation factor, 3' pre-RNA, subunit 3, 77kDa	1.66
11734141_at	GK5	glycerol kinase 5 (putative)	1.62
11725356_a_at	PRTFDC1	phosphoribosyl transferase domain containing 1	1.61
11740429_s_at	XRN1	5'-3' exoribonuclease 1	1.60
11758478_s_at	CDCA7	cell division cycle associated 7	1.60
11757980_s_at	EP400	E1A binding protein p400	1.58

Probe Set ID	Gene Symbol	Gene Title	Fold change (do vs d5)
11758221_s_at	ARRDC3	arrestin domain containing 3	1.57
11716689_s_at	GOLGA3	golgin A3	1.56
11726800_at	EBF1	early B-cell factor 1	1.56
11750022_a_at	LCORL	ligand dependent nuclear receptor corepressor-like	1.55
11745856_x_at	RNF145	ring finger protein 145	1.55
11753802_a_at	SRSF5	serine/arginine-rich splicing factor 5	1.53
11748460_a_at	RHOBTB1	Rho-related BTB domain containing 1	1.53
11753645_a_at	CFL1	cofilin 1 (non-muscle)	1.53
11732247_s_at	HNRNPC	heterogeneous nuclear ribonucleoprotein C (C1/C2)	1.52
11744492_x_at	SRSF5	serine/arginine-rich splicing factor 5	1.51
11723547_a_at	PEX1	peroxisomal biogenesis factor 1	1.51
11756162_s_at	PPAP2B	phosphatidic acid phosphatase type 2B	1.50
11720048_x_at	ARMCX1	armadillo repeat containing, X-linked 1	1.50
11724789_a_at	KIF3A	kinesin family member 3A	1.50
11715739_s_at	PPAP2B	phosphatidic acid phosphatase type 2B	1.49
11753646_x_at	CFL1	cofilin 1 (non-muscle)	1.48
11756063_x_at	SRSF5	serine/arginine-rich splicing factor 5	1.47
11754158_a_at	CFL1	cofilin 1 (non-muscle)	1.46
11725674_at	HINT3	histidine triad nucleotide binding protein 3	1.45
11727580_x_at	CSTF3	cleavage stimulation factor, 3' pre-RNA, subunit 3, 77kDa	1.45
11729215_x_at	PIGX	phosphatidylinositol glycan anchor biosynthesis, class X	1.45
11723548_x_at	PEX1	peroxisomal biogenesis factor 1	1.44
11752314_a_at	ATF7IP	activating transcription factor 7 interacting protein	1.44
11725579_s_at	BEND3	BEN domain containing 3	1.44
11716417_a_at	UNG	uracil-DNA glycosylase	1.43
11720047_a_at	ARMCX1	armadillo repeat containing, X-linked 1	1.43
11719593_at	RPRD2	regulation of nuclear pre-mRNA domain containing 2	1.43
11715693_s_at	CIRBP	cold inducible RNA binding protein	1.41
11728300_at	CCNE2	cyclin E2	1.41
11759450_x_at	DDI2	DNA-damage inducible 1 homolog 2 (S. cerevisiae)	1.39
11725420_at	GRLF1	glucocorticoid receptor DNA binding factor 1	1.38
11757323_x_at	TOP2B	topoisomerase (DNA) II beta 180kDa	1.38
11745411_a_at	TMX3	thioredoxin-related transmembrane protein 3	1.38
11745855_s_at	RNF145	ring finger protein 145	1.38
11748943_a_at	CHD4	chromodomain helicase DNA binding protein 4	1.38
11734103_a_at	FGGY	FGGY carbohydrate kinase domain containing	1.37
11751701_a_at	TMX3	thioredoxin-related transmembrane protein 3	1.37
11715531_at	PRPF8	PRP8 pre-mRNA processing factor 8 homolog (S. cerevisiae)	1.37
11747253_a_at	UNG	uracil-DNA glycosylase	1.37
11749528_a_at	CDCA7	cell division cycle associated 7	1.37
11716919_a_at	PDIA5	protein disulfide isomerase family A, member 5	1.36
200000_PM_s_at	PRPF8	PRP8 pre-mRNA processing factor 8 homolog (S. cerevisiae)	1.36
11747763_a_at	ADD1	adducin 1 (alpha)	1.36
11732768_at	RNF152	ring finger protein 152	1.36

Probe Set ID	Gene Symbol	Gene Title	Fold change (do vs d5)
11750255_x_at	ARID1A	AT rich interactive domain 1A (SWI-like)	1.36
11758140_s_at	CPSF6	cleavage and polyadenylation specific factor 6, 68kDa	1.36
11716455_at	RHOBTB3	Rho-related BTB domain containing 3	1.35
11720866_a_at	EIF2C1	eukaryotic translation initiation factor 2C, 1	1.35
11727595_at	KIAA2026	KIAA2026	1.35
11763439_s_at	HNRNPU	heterogeneous nuclear ribonucleoprotein U (scaffold attachment factor A)	1.35
11739640_at	DIP2A	DIP2 disco-interacting protein 2 homolog A (Drosophila)	1.35
11760192_s_at	TMEM68	transmembrane protein 68	1.35
11731480_a_at	SNRPB2	small nuclear ribonucleoprotein polypeptide B	1.34
11727594_a_at	KIAA2026	KIAA2026	1.34
11728301_a_at	CCNE2	cyclin E2	1.34
11737234_s_at	LOC162632 /// LOC220594 /// USP6	ubiquitin specific peptidase 6 (Tre-2 oncogene) pseudogene /// ubiquitin specific peptidase 6 (Tre-2 oncogene) pseudogene /// ubiquitin specific peptidase 6 (Tre-2 oncogene)	1.33
11758625_s_at	GSTA4	glutathione S-transferase alpha 4	1.33
11717060_a_at	DECR1	2,4-dienoyl CoA reductase 1, mitochondrial	1.32
11724491_at	NUDCD2	NudC domain containing 2	1.32
11727687_s_at	KCTD18	potassium channel tetramerisation domain containing 18	1.32
11728994_a_at	AZI2	5-azacytidine induced 2	1.31
11723200_s_at	HNRNPA3	heterogeneous nuclear ribonucleoprotein A3	1.31
11756291_a_at	CCDC53	coiled-coil domain containing 53	1.30
11763259_x_at	CFL1	cofilin 1 (non-muscle)	1.30
11723314_x_at	PXMP2	peroxisomal membrane protein 2, 22kDa	1.30
11757668_s_at	SERF1A /// SERF1B	small EDRK-rich factor 1A (telomeric) /// small EDRK-rich factor 1B (centromeric)	1.30
11734079_x_at	LONP2	lon peptidase 2, peroxisomal	1.29
11742679_s_at	HNRNPA2B1	heterogeneous nuclear ribonucleoprotein A2/B1	1.29
11741107_a_at	MRPS14	mitochondrial ribosomal protein S14	1.29
11721132_at	HCFC1	host cell factor C1 (VP16-accessory protein)	1.29
11741092_a_at	GPD2	glycerol-3-phosphate dehydrogenase 2 (mitochondrial)	1.28
11718457_at	STK11IP	serine/threonine kinase 11 interacting protein	1.28
11721835_s_at	TMEM14B	transmembrane protein 14B	1.27
11754638_a_at	USP30	ubiquitin specific peptidase 30	1.27
11720945_x_at	SNRPA1	small nuclear ribonucleoprotein polypeptide A'	1.27
11727026_a_at	NDUFB5	NADH dehydrogenase (ubiquinone) 1 beta subcomplex, 5, 16kDa	1.27
11716084_at	SF3B1	splicing factor 3b, subunit 1, 155kDa	1.27
11749307_x_at	CCNG1	cyclin G1	1.26
11726214_x_at	WWOX	WW domain containing oxidoreductase	1.26
11720520_s_at	PDE4DIP	phosphodiesterase 4D interacting protein	1.26
11737799_s_at	R3HDM1	R3H domain containing 1	1.25
11728646_at	NUCKS1	nuclear casein kinase and cyclin-dependent kinase substrate 1	1.25
11755368_a_at	MSH6	mutS homolog 6 (E. coli)	1.25
11741789_a_at	NDUFB6	NADH dehydrogenase (ubiquinone) 1 beta subcomplex, 6, 17kDa	1.24

Probe Set ID	Gene Symbol	Gene Title	Fold change (do vs d5)
11756967_x_at	SUCLG2	succinate-CoA ligase, GDP-forming, beta subunit	1.24
11745075_x_at	GSTA4	glutathione S-transferase alpha 4	1.24
11740462_a_at	C8orf40	chromosome 8 open reading frame 40	1.24
11731313_a_at	GCFC1	GC-rich sequence DNA-binding factor 1	1.24
11751219_x_at	GOLGA4	golgin A4	1.24
200014_PM_s_at	HNRNPC	heterogeneous nuclear ribonucleoprotein C (C1/C2)	1.22
11724079_s_at	E2F2	E2F transcription factor 2	1.21
11757636_x_at	ATP5L	ATP synthase, H+ transporting, mitochondrial Fo complex, subunit G	1.21
11754761_x_at	HMGN1	high-mobility group nucleosome binding domain 1	1.21
11756124_x_at	IKBKG	inhibitor of kappa light polypeptide gene enhancer in B-cells, kinase gamma	1.21
11757388_x_at	SHFM1	split hand/foot malformation (ectrodactyly) type 1	1.21
11755612_s_at	SNRPA1	small nuclear ribonucleoprotein polypeptide A'	1.20
11739087_a_at	MESDC2	mesoderm development candidate 2	1.19
11756337_x_at	HNRNPC	heterogeneous nuclear ribonucleoprotein C (C1/C2)	1.19
11757676_x_at	SHFM1	split hand/foot malformation (ectrodactyly) type 1	1.19
11758162_s_at	FDX1	ferredoxin 1	1.19
11749478_a_at	MCM3	minichromosome maintenance complex component 3	1.18
11724205_x_at	SUMO1	SMT3 suppressor of mif two 3 homolog 1 (S. cerevisiae)	1.18
11723357_x_at	SRSF2IP	serine/arginine-rich splicing factor 2, interacting protein	1.17
11748174_x_at	MCM3	minichromosome maintenance complex component 3	1.17
11717176_at	SNX27	sorting nexin family member 27	1.17
11757037_s_at	H3F3B	H3 histone, family 3B (H3.3B)	1.16
11724524_x_at	CDK5RAP2	CDK5 regulatory subunit associated protein 2	1.16
11756379_x_at	H3F3A /// LOC440926	H3 histone, family 3A /// H3 histone, family 3A pseudogene	1.14
11742997_x_at	MCM3	minichromosome maintenance complex component 3	1.14
11761622_x_at	TIPIN	TIMELESS interacting protein	1.13
11716369_x_at	SUMO2	SMT3 suppressor of mif two 3 homolog 2 (S. cerevisiae)	1.13
11736405_a_at	DNMT1	DNA (cytosine-5-)-methyltransferase 1	1.13
11723621_at	C7orf60	chromosome 7 open reading frame 60	1.13
11758459_s_at	API5	apoptosis inhibitor 5	1.12
11721679_a_at	RBM17	RNA binding motif protein 17	1.12
11721307_at	PHLDA1	pleckstrin homology-like domain, family A, member 1	1.09
11756233_a_at	AKIRIN2	akirin 2	1.09
11722606_s_at	CDC37L1	cell division cycle 37 homolog (S. cerevisiae)-like 1	1.08
11735695_a_at	ARF5	ADP-ribosylation factor 5	1.07
11758572_s_at	HELLS	helicase, lymphoid-specific	1.07
11727785_s_at	CACYBP	calcyclin binding protein	1.07
11722289_a_at	ZBTB43	zinc finger and BTB domain containing 43	1.06

Probe Set ID	Gene Symbol	Gene Title	Fold change (do vs d5)
11747496_x_at	USP19	ubiquitin specific peptidase 19	1.02
11754527_a_at	RQCD1	RCD1 required for cell differentiation1 homolog (S. pombe)	1.02
11742996_a_at	MCM3	minichromosome maintenance complex component 3	1.01
11725603_a_at	HOXA10 /// HOXA9	homeobox A10 /// homeobox A9	11.89
11716631_s_at	SERPINB2	serpin peptidase inhibitor, clade B (ovalbumin), member 2	10.82
11730130_at	HOXD10	homeobox D10	7.96
11723635_s_at	MMP3	matrix metallopeptidase 3 (stromelysin 1, progelatinase)	7.78
11735303_a_at	HOXA11	homeobox A11	7.75
11758100_s_at	C1S	complement component 1, s subcomponent	5.69
11757367_s_at	HSPA6 /// HSPA7	heat shock 70kDa protein 6 (HSP70B') /// heat shock 70kDa protein 7 (HSP70B)	4.93
11744770_a_at	HOXA11	homeobox A11	4.70
11729385_at	FOXF1	forkhead box F1	4.61
11742701_x_at	C1R	complement component 1, r subcomponent	4.29
11740290_a_at	HOXC6	homeobox C6	4.27
11742699_a_at	C1R	complement component 1, r subcomponent	3.92
11729020_at	ZNF804A	zinc finger protein 804A	3.71
11758071_s_at	SULF1	sulfatase 1	3.28
11747162_a_at	FLT1	fms-related tyrosine kinase 1 (vascular endothelial growth factor/vascular permeability factor receptor)	2.91
11757865_a_at	GADD45B	growth arrest and DNA-damage-inducible, beta	2.67
11742688_s_at	HIST2H2AA3 /// HIST2H2AA4	histone cluster 2, H2aa3 /// histone cluster 2, H2aa4	2.33
11747820_x_at	UPP1	uridine phosphorylase 1	2.22
11727867_a_at	CLEC3B	C-type lectin domain family 3, member B	2.07
11719388_x_at	MAFK	v-maf musculoaponeurotic fibrosarcoma oncogene homolog K (avian)	1.95
11745531_a_at	MARCH3	membrane-associated ring finger (C3HC4) 3	1.91
11742657_x_at	HIST2H2AA3 /// HIST2H2AA4	histone cluster 2, H2aa3 /// histone cluster 2, H2aa4	1.90
11733725_a_at	CFB	complement factor B	1.89
11758020_s_at	EIF5	eukaryotic translation initiation factor 5	1.88
11742287_a_at	CHAC1	ChaC, cation transport regulator homolog 1 (E. coli)	1.72
11725074_a_at	FAM126A	family with sequence similarity 126, member A	1.70
11727883_a_at	AP3M2	adaptor-related protein complex 3, mu 2 subunit	1.59
11717548_a_at	BTBD10	BTB (POZ) domain containing 10	1.58
11726566_a_at	EIF4G1	eukaryotic translation initiation factor 4 gamma, 1	1.58
11746235_a_at	LIN37	lin-37 homolog (C. elegans)	1.54
11743041_a_at	STIP1	stress-induced-phosphoprotein 1	1.53
11755709_s_at	LARP6	La ribonucleoprotein domain family, member 6	1.50
11718276_x_at	IFRD2	interferon-related developmental regulator 2	1.49
11724307_x_at	ORAOV1	oral cancer overexpressed 1	1.49
11748596_a_at	KLHL2	kelch-like 2, Mayven (Drosophila)	1.49

Probe Set ID	Gene Symbol	Gene Title	Fold change (do vs d5)
11732434_at	ZNF250	zinc finger protein 250	1.48
11758547_s_at	EML1	echinoderm microtubule associated protein like 1	1.47
11755876_a_at	IFRD2	interferon-related developmental regulator 2	1.47
11733264_a_at	EML1	echinoderm microtubule associated protein like 1	1.47
11755281_a_at	TGFBI	transforming growth factor, beta-induced, 68kDa	1.47
11756564_a_at	AUP1	ancient ubiquitous protein 1	1.45
11752509_s_at	PSAP	prosaposin	1.45
11716799_at	FADD	Fas (TNFRSF6)-associated via death domain	1.44
11720523_at	RRP9	ribosomal RNA processing 9, small subunit (SSU) processome component, homolog (yeast)	1.43
11739198_a_at	DDX52	DEAD (Asp-Glu-Ala-Asp) box polypeptide 52	1.42
11725591_a_at	SPATA2	spermatogenesis associated 2	1.42
11715902_a_at	DDX23	DEAD (Asp-Glu-Ala-Asp) box polypeptide 23	1.42
11746438_a_at	SHMT2	serine hydroxymethyltransferase 2 (mitochondrial)	1.41
11742925_a_at	C11orf59	chromosome 11 open reading frame 59	1.41
11715445_a_at	DNAJB1	DnaJ (Hsp40) homolog, subfamily B, member 1	1.41
11722199_at	ADAM12	ADAM metallopeptidase domain 12	1.40
11736280_at	SLC22A3	solute carrier family 22 (extraneuronal monoamine transporter), member 3	1.39
11720313_a_at	ATP6V0B	ATPase, H+ transporting, lysosomal 21kDa, V0 subunit b	1.37
11743066_s_at	PTDSS1	phosphatidylserine synthase 1	1.37
11734550_x_at	TGFBI	transforming growth factor, beta-induced, 68kDa	1.37
11719841_s_at	PHLDA3	pleckstrin homology-like domain, family A, member 3	1.36
11753017_s_at	HSPD1	heat shock 60kDa protein 1 (chaperonin)	1.35
11730930_a_at	IKBKB	inhibitor of kappa light polypeptide gene enhancer in B-cells, kinase beta	1.35
11750213_a_at	ADPRHL2	ADP-ribosylhydrolase like 2	1.33
11739458_at	SYNC	syncoilin, intermediate filament protein	1.32
11738829_x_at	C1orf109	chromosome 1 open reading frame 109	1.32
11739615_at	CD3EAP	CD3e molecule, epsilon associated protein	1.31
11720969_a_at	GART	phosphoribosylglycinamide formyltransferase, phosphoribosylglycinamide synthetase, phosphoribosylaminoimidazole synthetase	1.30
11751697_a_at	NAA50	N(alpha)-acetyltransferase 50, NatE catalytic subunit	1.30
11753923_at	LOC401093	hypothetical LOC401093	1.30
11716983_at	CDC34	cell division cycle 34 homolog (S. cerevisiae)	1.29
11719280_a_at	NAA10	N(alpha)-acetyltransferase 10, NatA catalytic subunit	1.29
11736675_a_at	SNRPB	small nuclear ribonucleoprotein polypeptides B and B1	1.29
11749555_a_at	MAP2K1	mitogen-activated protein kinase kinase 1	1.28
11750992_x_at	SHMT2	serine hydroxymethyltransferase 2 (mitochondrial)	1.27
11746872_a_at	COL1A1	collagen, type I, alpha 1	1.27
11724373_a_at	GSK3A	glycogen synthase kinase 3 alpha	1.27
11720468_x_at	DPAGT1	dolichyl-phosphate (UDP-N-acetylglucosamine) N-acetylglucosaminephosphotransferase 1 (GlcNAc-1-P transferase)	1.24

Probe Set ID	Gene Symbol	Gene Title	Fold change (do vs d5)
11716218_s_at	PRKAB1	protein kinase, AMP-activated, beta 1 non-catalytic subunit	1.24
11754105_x_at	SNRPB	small nuclear ribonucleoprotein polypeptides B and B1	1.24
11726365_a_at	ERICH1	glutamate-rich 1	1.24
11753649_s_at	SRSF3	serine/arginine-rich splicing factor 3	1.23
11755048_a_at	MED22	mediator complex subunit 22	1.23
11751675_s_at	AK2	adenylate kinase 2	1.23
11754070_a_at	SSNA1	Sjogren syndrome nuclear autoantigen 1	1.22
11758809_at	RRAGC	Ras-related GTP binding C	1.22
11760170_x_at	SNRPB	small nuclear ribonucleoprotein polypeptides B and B1	1.21
11719398_s_at	RRAGC	Ras-related GTP binding C	1.21
11715388_s_at	CDKN1A	cyclin-dependent kinase inhibitor 1A (p21, Cip1)	1.21
11719392_a_at	RNF14	ring finger protein 14	1.20
11743468_at	DKC1	dyskeratosis congenita 1, dyskerin	1.19
11716651_a_at	UBE2Z	ubiquitin-conjugating enzyme E2Z	1.19
11745884_a_at	UBE2Z	ubiquitin-conjugating enzyme E2Z	1.19
11747276_a_at	AKAP1	A kinase (PRKA) anchor protein 1	1.19
11721312_a_at	ATOX1	ATX1 antioxidant protein 1 homolog (yeast)	1.18
11757499_s_at	C10orf26	chromosome 10 open reading frame 26	1.17
11749300_x_at	WDR77	WD repeat domain 77	1.17
11751353_a_at	RRAGC	Ras-related GTP binding C	1.16
11739106_a_at	TMEM33	transmembrane protein 33	1.15
11715728_a_at	ITGB1	integrin, beta 1 (fibronectin receptor, beta polypeptide, antigen CD29 includes MDF2, MSK12)	1.13
11756187_s_at	RPA2	replication protein A2, 32kDa	1.13
11750638_a_at	SF3A1	splicing factor 3a, subunit 1, 120kDa	1.12
11744136_at	CADM4	cell adhesion molecule 4	1.11
11756885_a_at	ATAD2	ATPase family, AAA domain containing 2	1.11
11740896_s_at	C17orf91	chromosome 17 open reading frame 91	1.11
11731068_s_at	FIGNL1	fidgetin-like 1	1.10
11757443_s_at	C18orf55	chromosome 18 open reading frame 55	1.10
11726238_s_at	TRIM36	tripartite motif-containing 36	1.09
11719636_a_at	NUP153	nucleoporin 153kDa	1.08
11716354_a_at	NDUFA11	NADH dehydrogenase (ubiquinone) 1 alpha subcomplex, 11, 14.7kDa	1.06
11758558_s_at	ATP2A2	ATPase, Ca++ transporting, cardiac muscle, slow twitch 2	1.05
11731826_at	ZNF425	zinc finger protein 425	1.03
11754477_x_at	GNL1	guanine nucleotide binding protein-like 1	1.03
11745202_a_at	RMI1	RMI1, RecQ mediated genome instability 1, homolog (S. cerevisiae)	1.02
11744541_a_at	CXCR7	chemokine (C-X-C motif) receptor 7	1.02
11756674_s_at	STRBP	spermatid perinuclear RNA binding protein	1.01
11733147_at	ZFP161	zinc finger protein 161 homolog (mouse)	1.01
11722897_a_at	REV1	REV1 homolog (S. cerevisiae)	1.01
11746556_a_at	SLBP	stem-loop binding protein	1.01
11721305_a_at	PHLDA1	pleckstrin homology-like domain, family A, member 1	1.00